applied sciences

MDPI

Review

Non-Uniform Temperature Fields and Effects of Steel Structures: Review and Outlook

Wucheng Xu, Deshen Chen * and Hongliang Qian

Department of Civil Engineering, Harbin Institute of Technology at Weihai, Weihai 264209, China; 18s030198@stu.hit.edu.cn (W.X.); qianhl@hit.edu.cn (H.Q.)

* Correspondence: chends@hit.edu.cn; Tel.: +86-6315-687-955

Received: 22 June 2020; Accepted: 27 July 2020; Published: 30 July 2020

check for updates

Abstract: Due to the dynamic coupling effects of solar radiation, longwave radiation, convective heat transfer, shadows, and other factors, the temperature field and effect of steel structures are significantly non-uniform, differing from traditional concepts that regard the temperature variation of steel structures as a slow and uniform progress. This difference can hinder the correct understanding of the thermal behavior of steel structures and ignore some potential safety hazards. This paper provides a review of the studies for the non-uniform temperature field and effect of steel structures, and presents some outlooks on future developments on the basis of the current research situation. A summary of research on the temperature field and effect of space structures, bridges and radio telescopes initially establishes the basic cognitive framework for this field. In addition, then, the basic principles of the numerical simulation of temperature fields are introduced through heat transfer mechanism, and the experimental test methods of temperature and its effects are described based on typical test cases. Finally, with a view to the future, some suggestions and opinions are provided in consideration of deficiencies in the current research status. This paper hopes to provide some valuable references for future research in this field through research summary, method introduction and outlook.

Keywords: non-uniform temperature field; non-uniform temperature effect; numerical simulation; experimental test; steel structure

1. Introduction

Steel structures are widely used in civil and industrial architecture for their advantages of high strength, light weight and strong deformation resistance [1]. With the development of design methods and construction technologies, the structural forms of steel structures are becoming more and more complex, and their engineering scale is growing; meanwhile, they are very sensitive to temperature variation. Within the lifecycle of a steel structure, which includes the construction and service periods, due to the dynamic coupling effects of solar radiation, longwave radiation, convective heat transfer, shadows, and other factors, its temperature field and effect will have significant time variations and non-uniformity [2,3]. However, the traditional and familiar design methods regard the temperature variation of steel structures to be a slow and uniform process [4–6], mainly considering seasonal temperature variations and ignoring the influence of other environmental factors, which leads to differences between calculation results and the practical situation of temperature fields and effects of steel structures.

During the construction period, steel structures are exposed to solar radiation, and their non-uniform temperature distributions can cause complex temperature effects, which will directly affect engineering construction quality and structural closure accuracy [7,8], and the possible construction defects can even lead to potential safety hazards [9]. During the service period, the temperature fields of steel structures under outdoor or transparent rooves are also non-uniform, and the temperature effects caused by this not only reduce the structural working performance, but can even result in some damage [10]. An outdoor steel arch structure in Inner Mongolia was formed in summer, under conditions of strong solar radiation; the increase in structural temperature relative to air temperature as a result of environmental factors was not considered in the design and construction stage. After a sudden drop in air temperature in winter, the variation in air temperature and the fact that the increase in structural temperature had been ignored resulted in a great negative temperature difference, leading to the cracking of the welding seam area [11]. Some studies have shown that the adverse effects of temperature on the fatigue of orthotropic steel decks and the dynamic characteristics of long-span bridges cannot be ignored [12,13], and a research report on the US 311 Bridge also refers to the detailed analysis of the temperature effect [14]. The non-uniform temperature effect is one of the important factors affecting the working performance of the Five-Hundred-Meter Aperture Spherical Telescope, and the structural calculation in the design stage shows that thermal deformation directly and significantly affects the surface accuracy of the reflector during the service period [15]. To date, the non-uniform temperature fields and effects of steel structures have been widely examined as important research topics in academic and engineering circles. However, the study of temperature field and effect is usually complex because of its multi-disciplinary nature, incorporating mechanics, heat transfer, meteorology, astronomy, computer graphics, etc. Therefore, it is necessary to summarize the research in this field and provide some valuable references.

In this paper, previous studies of the non-uniform temperature field and effect of steel structures are first summarized, which mainly relate to space structures, bridges and radio telescopes. It is helpful to understand the current research situation in order to perceive opportunities for future development. According to the heat transfer process, the basic principle of temperature field simulation is presented; three common calculation models of solar radiation are reviewed, along with their history and formulas, and some representative expressions of convective heat transfer coefficient are also provided. Typical test cases regarding the temperature field and effects of steel structures are listed, on the basis of which test equipment and schemes are summarized. Finally, based on the above summary, improvements and developments of studies in this field are explored with a view to the future.

2. Previous Studies

Previous studies on the non-uniform temperature field and effects of steel structures have mainly focused on space structures, bridges and radio telescopes.

2.1. Space Structures

Space structures are rather sensitive to temperature variations because of their high degrees of static indeterminacy [16–18]. Therefore, it is necessary for structural design and construction calculations to study the practical temperature distributions and variations in space structures.

As one important prerequisite, the study of the temperature distribution laws of steel members is helpful for determining the temperature field of space structures. Many experiments have shown that the temperature of steel members along the length and thickness directions can be assumed to be uniform, while the temperature distribution of member sections along the horizontal and vertical directions is significantly non-uniform [19–21]. There are many factors that affect the non-uniform temperature distribution of steel members, such as solar radiation intensity, ambient wind speed, section size, and the surface coating of the steel member [22]. Chen continuously monitored the temperature field of I-shaped steel, a rectangular tube, and a circular tube over a 90-day test period, lasting from July to September in 2015 [23]. Based on the test results, the non-uniformity of the temperature distribution was positively and negatively correlated with solar radiation intensity and ambient wind speed, respectively. Under identical conditions, the temperature distribution of small section members was mainly controlled by thermal conduction, and the maximum temperature difference of small sections of circular tube (76 × 3 mm) was only around 4 °C, but the self-shadow influence of the member on temperature distribution increased gradually with the increase in section size, and the maximum temperature difference of larger sections of circular tube (219 × 5 mm) could reach more than 16 °C. Liu tested the temperature of steel plates with different surface coatings under sunlight [24]. The darker the surface coating, the higher the temperature of the steel plate, and the maximum temperature difference between steel plates with different surface coatings was up to 19.3 °C in summer. Chen also studied the temperature effects of steel members under rigid and hinged constraints induced by solar radiation through on-site monitoring and numerical analysis [25]. The thermal deformation of all specimens, which included I-shaped steel, a rectangular tube, and a circular tube, was relatively small and less than 1/3000 of their spans. However, the thermal stress of steel members induced by solar radiation was considerable, the stress distribution was obviously non-uniform, and the maximum temperature stresses of all specimens under rigid and hinged constraints reached up to 67 MPa and 58 Mpa, respectively. This indicates that the non-uniform temperature stress of steel members induced by solar radiation needs to be studied further and considered in structural design. Based on the analysis of long-term test data, Chen found one positive correlation between the average temperature and the average temperature stress of steel members, and given the corresponding linear coefficient according to the type of specimens and constraints.

Considering the large number of members, the non-uniform temperature field of space structures is more complex than that of individual members. During the construction period, space structures are directly exposed to solar radiation with a significant structural temperature difference. Based on long-term monitoring data, the maximum temperature of the steel lattice structure of the Yujiabu Railway Station Building under strong solar radiation is more than 18 °C [26,27]. There are great differences between the solar transmittance of different roof materials, such as glass, light steel and ETFE membrane [28]. When the roof is composed of several materials, the non-uniformity of the temperature field of space structures that are in service is more significant than that of those under construction. The roof of the indoor water recreation project Tien Rice Cube is composed of glass and light steel, and the temperature of steel members under glass roof is significantly higher than that under light steel rooves, with a structural temperature difference of 24 °C at noon in summer [29]. A large number of studies for practical engineering show that the temperature fields of space structures are significantly non-uniform [30–32], and the non-uniformity is positively correlated with the intensity of solar radiation [8]. The temperature effects of space structures, which includes thermal stress and deformation, caused by non-uniform temperature fields are more significant than those under traditional uniform temperature loads, and the high degree of deformation directly affects the structural construction quality [33]. The non-uniform thermal load is obtained on the basis of the simulated temperature field, and the maximum member stress and maximum nodal displacement of the reticulated shell structure of Caofeidian Coal Storage under non-uniform thermal loads are 80.4 mm and 68.9 MPa, which are 42.65% and 55.21% higher than the calculation results when considering atmosphere temperature variation only [34]. The Chiping Gymnasium is a typical suspen-dome with a stacked arch structure, its non-uniform temperature field under solar radiation has a remarkable effect on the hoop cable force, and the error between the practical and design pre-stressing force of the hoop cable can reach up to 212% due to non-uniform temperature variation during the construction period [35,36].

In summary, regardless of whether considering the structure level or the member level, the temperature of space structures is non-uniform. Compared with uniform temperature fields, which only consider variations in atmospheric temperature in the traditional concept, the temperature effects of space structures caused by practical non-uniform temperature fields are more remarkable, and may be more unfavorable to the construction progress and working performance of steel structures. Therefore, the temperature effects caused by non-uniform temperature variations should be considered in the construction organization and structural design of space structures, and some specifications currently indicate a design method for non-uniform temperature loads in single steel members [37,38].

2.2. Bridges

There are many factors leading to the complex temperature fields in bridge structures, such as solar radiation, atmospheric temperature, and wind speed [39,40]. The significant structural thermal effect is caused by the complex temperature fields of bridges, which can result in potential safety hazards [41,42]. The study of the temperature fields and effects of bridges is important and valuable for ensuring their safety during operation.

The temperature fields of steel truss bridges under solar radiation is significantly non-uniform due to the effect of the self-shadow of members and the shadow between members, and this non-uniformity is not only reflected in the temperature difference between steel truss members, but also in the temperature differences within the cross-sections of each steel truss member [43,44]. Through the comparative analysis of test results from the Dashengguan Yangtze Bridge, the static strain variations of steel truss members are mainly caused by temperature and trains, and the correlation between the temperature field and the remaining static stress shows good linear characteristics after removing train-induced static strain [45]. The large horizontal rotation angles at the beam ends of railway bridges can lead to the variation of track geometry state and damage of rail fastening systems [46]. Based on the long-term monitoring data of several railway steel truss bridges, the non-uniform temperature distribution of steel trusses is the key factor leading to the horizontal rotation angle, especially for the transverse temperature difference between the bottom chord trusses and the transverse temperature difference between the top chord trusses [47,48].

For steel box girders in bridge structures, the temperature along its longitudinal direction is relatively uniform, but the temperature distribution through the cross-section is significantly non-uniform due to the shadow effect [49]. Based on Eurocode 1 for thermal actions [50], non-uniform temperature distributions through the cross-section can be divided into a uniform temperature component, a vertical temperature difference component, and a horizontal temperature difference component. On the basis of the temperature field monitoring data of the Normandy Bridge's steel box girder over 34 months, Lucas discovered that there was a difference, which was caused by solar radiation, between the daily maximums of the uniform temperature component and the air temperature, but that their daily minima were in good agreement [51,52]. Many studies have shown that vertical temperature difference is usually significantly higher than horizontal temperature difference in normal cases; therefore, only the vertical temperature difference must be considered in these cases. The functions of quintic parabola, quadratic and cubic polylines have been used to describe the vertical temperature gradient curve modes for steel box girders in various studies [53–55]. However, the large horizontal temperature difference must also be considered in particular cases; for example, it reaches up to a maximum of 18 °C for the Humber Bridge based on the measured data [56]. Six horizontal temperature difference models were proposed by Ding for the top plate of steel box girders on the basis of the monitoring data from the Runyang Cable-Stayed Bridge [57]. Throughout the life cycle of steel box girders, they are under outdoor conditions and are directly exposed to solar radiation; thus, the adverse effects of non-uniform temperature distribution are not only reflected during the construction period, but also during the service period. The steel box girders in bridge structures are usually assembled from several prefabricated sections. During the construction process, the non-uniform temperature distributions can result in the thermal deformation of prefabricated sections, which can lead to dislocations between the two prefabricated sections to be connected, which may directly affect closure accuracy and construction quality [58]. Wang applied finite element software to simulate the non-uniform temperature field of curved steel box girders in the Shangtang Bridge, and used the simulated temperature field as the thermal load. Based on the overturning stability analysis, during the service period, the steel box girder bridge was rather likely to overturn under a combination of the effects of non-uniform temperature, gravity and vehicle loads [59].

In cable-stayed bridges, as the important tension members, the working state of the stay cables directly determines the structural performance of the bridge. The temperature and displacement of main cable were obtained for several years through the health monitoring system of the Tsing

Ma Bridge, and the temperature of the main cable was usually slightly higher than the ambient air temperature by 2–3 °C, and the vertical displacement of the main cable was remarkable, with a daily variation of around 220 mm, but its longitudinal displacement was much smaller, with a daily variation of around 40 mm [60,61]. Zhou studied the cable force variation caused by temperature combined with the measurement results of the Shanghai Yangtze River Bridge and theoretical analysis, and proposed a formula for predicating cable force [62]. Yang calculated the cable force of the Anqing Yangtze River based on GPS data, and found that there was one obvious negative correlation between the measured structural temperature and cable force [63]. Wang analyzed the extreme weather during the monitoring period of the Puxi Bridge and simulated its temperature field under extreme weather conditions, and further designed the thermal load combinations for the simulation of extreme weather events; the calculation results show that the maximum variation of the cable fore under extreme weather reached up to 144.44 kN [42].

Overall, the temperature fields of steel structures in bridges under the combined action of various environmental factors shows strong non-uniformity and time-variance, and adverse temperature-induced effects are significant, such as the large horizontal rotation angles at the beam ends, risk of overturning and sharp variations in cable force, which can lead to the potential safety hazards. It is suggested that these adverse temperature effects be a focus in bridge design and the formulation of relevant countermeasures; for example, Wang proposed three methods for solving the overturning problem of steel box girders: adding balance weight in the support regions, adjusting the placement of bearings, and installing tensile bearings [59].

2.3. Radio Telescopes

Around the world, a large number of radio telescopes have been built in order to explore the cosmic environment [64], and great progress has been made in astronomy with the help of radio telescopes in recent decades [65,66]. The radio radiation from outer space is gathered through the reflection of the main reflector and the subreflector, and the gathered radiation is received through a feed. To ensure the quality of the reflection process, the reflectors are designed in the form of specific shapes, such as paraboloid and spherical surfaces. However, the reflectors will produce deformation under a combination of the effects of temperature, gravity and wind load, leading to differences between their practical and designed shape that may directly affect the working performance of the telescope [67,68]. Therefore, studying the temperature fields and temperature deformations of radio telescopes is important for the thermal design and control.

Fixed radio telescopes are usually designed with the incorporation of super-large-aperture reflectors, such as the Five-hundred-meter Aperture Spherical Telescope (FAST) [69] and the Arecibo Radio Telescope [70]. The influence of temperature deformation on the structure of telescopes with high precision and large apertures is significant, and is usually regarded as an important research component for structural design. On karst depression of Guizhou, the Five-hundred-meter Aperture Spherical Telescope (FAST) was built with a cable-net structure as a supporting system [71]. In the structural design stage, the temperature field of the FAST was simulated on the basis of reasonable assumptions [15]. Due to the shadow effect of the surrounding mountain block [72], the simulated temperature field was significantly non-uniform during the daytime. In particular, during a typical summer day (15 July), the structural temperature difference was more than 10 °C through most of the daytime. In order to further study the temperature deformation of the FAST, the simulation results of temperature fields were used as the thermal load [73]. Based on the calculation results, the root mean square of the fitting error for the reflector geometry caused by temperature deformation can reach up to a maximum value of 2.5 mm all year around, which is 50% of the allowable overall error for ensuring surface precision, and the fitting error of the reflector local position caused by non-uniform temperature variation is much larger. Through further analysis of fitting errors and the working state of radio telescopes, it is recommended that radio observations be made at sunrise, when the temperature field of the FAST is relatively uniform [74].

Movable radio telescopes are a common design form at present, and can ensure real-time tracking through the rotation of the reflector [75]. Since the 1980s, Greve has studied the thermal behavior of the IRAM-30 m Telescope, and proposed systematic numerical methods for calculating the temperature fields and effects of movable telescope structures [76–78]. The construction materials of movable radio telescopes mainly include steel and aluminum, which have good thermal conductivity and large specific heat capacity, so the effects of solar radiation and wind on the temperature fields of telescopes should be considered, and the adverse effects of temperature deformation on reflector surface precision and pointing accuracy must be effectively controlled in order to guarantee good observational performance [79]. Qian studied the temperature field and solar cooker effect of the Shanghai 65 m Radio Telescope under different working conditions through model experiments and numerical simulations for several years [80,81]. The non-uniformity of the Shanghai 65 m Radio Telescope's temperature filed under solar radiation is reflected in the back-up and reflector structure, and the non-uniform structural temperature deformation leads to the geometric shape of the telescope during its service period being different from its designed shape, resulting in possible observation errors [82]. The solar cooker effect refers to the phenomenon of sunlight gathering on the main reflector and subreflector, which can cause rather high temperatures, and huge temperature deformations in localized positions on the reflector [83]. Based on finite element analysis, the maximum temperatures of the main reflector and subflector of the Shanghai 65 m Radio Telescope under solar radiation were up to 44.5 °C and 144.9 °C during the daytime, indicating that the solar cooker effect on the subreflector is more significant and nonnegligible [84]. Thus, on the basis of an analysis of these results, unfavorable working states and times should be avoided as much as possible in the process of radio observation when using movable radio telescopes [85]. In addition, the temperature fields and effects of other movable radio telescopes have also been studied through the use of measurements or simulations, including the RT-70 Telescope [86], the Green Bank Telescope [87], and the Nobeyama 45 m Telescope [88,89].

Aperture synthesis radio telescopes, which consists of several fixed and movable radio telescopes, not only provide a large signal receiving area, but also avoid the construction difficulties of large-aperture radio telescope; these include the Square Kilometer Array [90] and the Atacama Large Millimeter/submillimeter Array [91]. Chen measured the temperature field of the main reflector and subreflector of one 3 m aperture radio telescope model continuously for two months [92,93], the experimental results showed that the solar cooker effect and non-uniform temperature distribution of the main reflector and subreflector were also remarkable even for small aperture radio telescopes, implying that temperature deformation and surface precision error cannot be ignored. The large number of radio telescopes that make up synthetic aperture telescopes may be under different working states, where the superposition effect of possible observation errors caused by thermal deformation could be considerable.

To summarize, experimental and numerical studies show that the temperature field of radio telescopes under solar radiation is obviously non-uniform, and the corresponding solar cooker effect is also nonnegligible; the temperature deformation caused by non-uniform temperature variation can directly affect the surface precision and pointing precision of radio telescopes, resulting in possible observation errors. To ensure the observation accuracy, important observation tasks should be carried out at appropriate working times, and avoiding unfavorable working states of the radio telescope; meanwhile, the adoption of some effective measures have also been suggested, such as enhancement of ambient air flow [94].

3. Research Method

The research of non-uniform temperature fields and effects of steel structures involves multiple disciplines, including mechanics, heat transfer, meteorology, computer graphics, etc. Therefore, it is difficult to obtain accurate analytical solutions based on the complex heat boundary conditions and simple heat conduction equations. At present, research methods mainly include numerical simulation and experimental testing.

3.1. Numerical Simulation

The simulation results of the temperature field of a steel structure are usually used as the thermal loads for the numerical calculation of its temperature effects, so the numerical accuracy of the temperature effect depends greatly on the accuracy of the simulation results of the temperature field. Therefore, the numerical simulation of the temperature field is introduced in this paper.

The temperature field of steel structures is determined by internal heat conduction and external heat exchange. The theory of heat conduction is relatively mature, and it can be calculated directly from the material properties using finite element software. Take I-shaped steel for example; Figure 1 shows the heat exchange between the steel structure and the external environment, which is divided into radiative heat transfer and convective heat transfer. Radiative heat transfer is the process of heat transfer between objects in the form of electromagnetic waves, and includes solar radiation and longwave radiation. Longwave radiation, which mainly consists of sky radiation and ground radiation, can be calculated by Equation (1) [95]. F_{wg} and F_{ws} in Equation (1) can be calculated by Equations (2) and (3), respectively.

$$q_l = \varepsilon_f \sigma \left[F_{wg}\left(T_g^4 - T^4\right) + F_{ws}\left(T_{sky}^4 - T^4\right) \right] \tag{1}$$

$$F_{wg} = (1 - cos\alpha)/2 \tag{2}$$

$$F_{ws} = (1 + cos\alpha)/2 \tag{3}$$

where q_l is longwave radiation (W/m^2); ε_f is the ratio of the radiation emitted by a surface; $\sigma = 5.67 \times 10^{-8}$ W/$\left(\text{m}^2\cdot\text{K}^4\right)$ is the Stefan–Boltzmann constant; F_{wg} is the view factor from the surface to the ground; F_{ws} is the view factor from the surface to the sky; T_g is the ground temperature (K); T_s is the effective temperature of sky (K), which can be calculated by $T_{air} - 6$K; T_{air} is the air temperature (K); T is the temperature of the surface (K); and α is the tilt angle of the surface from horizontal.

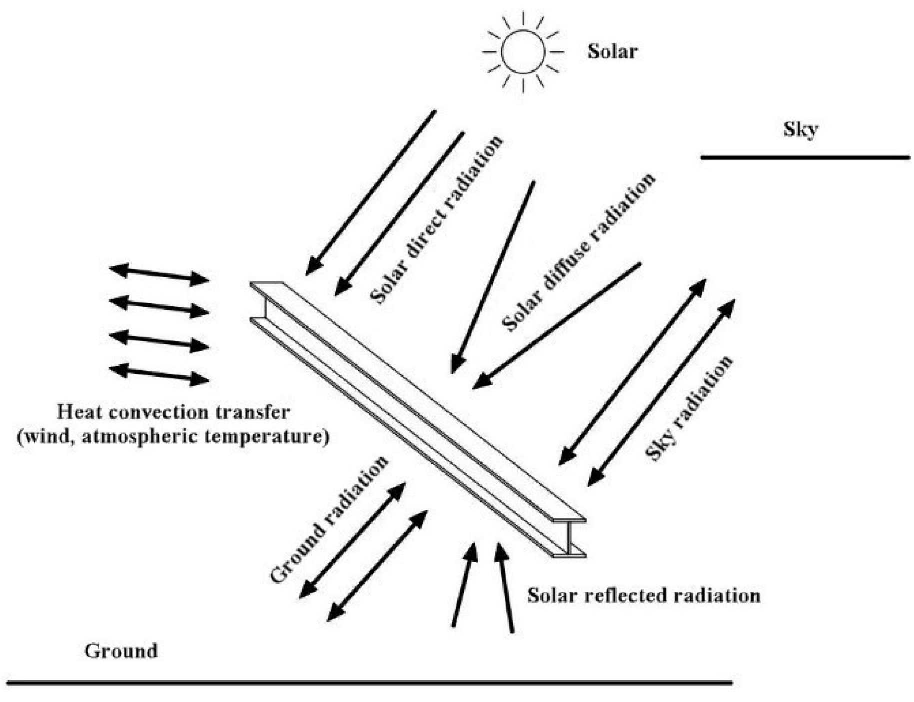

Figure 1. Heat transfer between the steel structure and external environment using I-shaped steel as an example.

The solar radiation absorbed by the surface of the steel structure can be divided into direct radiation, diffuse radiation, and reflected radiation. Direct solar radiation refers to the radiation emitted by the sun that is directly transmitted to the surface of the steel structure in the form of parallel rays. Partial solar radiation from the atmosphere reaches the steel structure surface at different angles owing to the scatter action of gas, dust and aerosol in the atmosphere, and this radiation is known as diffuse solar radiation. Due to the reflection effect from other objects, especially from the ground, the reflected direct and diffuse solar radiation absorbed by the steel structure surface is reflected solar radiation, which can be calculated directly on the basis of the reflectivity of object surfaces and geometric mathematics. However, the direct and diffuse solar radiation are very complex and are related to many factors, such as atmospheric transparency, solar altitude angle, altitude, etc.; the most commonly used models for their calculation include the ASHARE model, the Hottel model, and the power exponent model. The three basic components of solar radiation are shown in Figure 2.

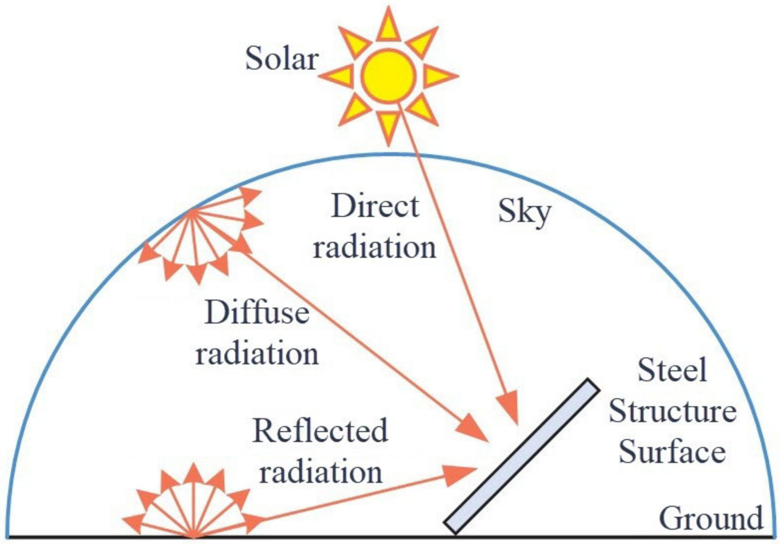

Figure 2. Three basic components of solar radiation.

As the clear sky model recommended by the American Society of Heating, Refrigerating, Air Conditioning Engineers, the ASHARE model was originally developed by Moon [96], and later was modified by Threlkeld [97]. The radiation calculation formulas of the model are as follows [98]:

$$I_{bn} = Ae^{-B/sinh} \tag{4}$$

$$I_{dh} = CI_{bn} \tag{5}$$

where I_{bn} is the direct solar radiation intensity on the surface normal (W/m^2), I_{dh} is the diffuse solar radiation intensity on the horizontal surface (W/m^2), h is the solar altitude angle, and A, B, C are the apparent solar irradiation, atmospheric extinction coefficient and diffuse radiation factor, respectively. The three empirical coefficients are all functions of monthly variation and are obtained on the basis of the measured data for solar radiation in the United States.

The Hottel model is a clear sky model suitable for conditions with visibility higher than 23 km and altitude lower than 2500 m. In the Hottel model, the transmittance of direct solar radiation (τ_b) and the transmittance of diffuse solar radiation (τ_d) are applied in order to calculate solar radiation, as shown in Equations (6) and (7).

$$I_{bh} = \tau_b I_0 \tag{6}$$

$$I_{dh} = \tau_d I_0 \tag{7}$$

where I_{bh} is the direct solar radiation intensity on the horizontal surface (W/m^2), and I_0 is the solar radiation intensity at the outside tangent plane of the atmosphere (W/m^2).

In 1976, Hottel [99] established the model and proposed a formula for calculating the transmittance of direct solar radiation based on the altitude and solar altitude angle; this formula is $\tau_b = a_0 + a_1 e^{-k/sinh}$. a_0, a_1, k are all empirical coefficients in consideration of climate types. The transmittance of diffuse solar radiation is usually calculated using the formula $\tau_d = 0.271 - 0.294\tau_b$, proposed by Liu and Jordan [100] in 1960.

The direct solar radiation decreases exponentially as sunlight passes through the atmosphere. When studying the temperature stress of bridge structures under solar radiation, Kehlbeck [101] followed the Bouguer–Lambert Law and provided method for calculating the direct solar radiation at the earth's surface using the power exponent model.

In 1983, Dilger [102] established a systematic power exponent model to calculate direct solar radiation, and this model can be represented as the following formula:

$$I_{bn} = k_T I_0 \tag{8}$$

$$k_T = 0.9^{mt_u} \tag{9}$$

$$m = k_a / sin(h + 5^\circ) \tag{10}$$

where k_T is the transmittance factor, which expresses the scatter of the light in a pure atmosphere, as well as the absorption of certain wavelengths by the atmosphere; t_u is the atmospheric turbidity factor, which expresses the attenuation of direct solar radiation under different atmospheric conditions; m is the air mass factor, which gives the relative path length of the radiation through the atmosphere; and k_a is relative atmospheric pressure.

Since then, many scholars have used Dilger's method to calculate direct solar radiation, including Elbadry [103], Chen [104], Zhou [105], etc.

Compared with the other two models, the ASHARE model is the most complex, and its three empirical coefficients require long-term meteorological observation data from different sites to be obtained in order to apply them to the corresponding areas. In addition, the atmospheric turbidity factor also needs to be obtained through meteorological information from the corresponding areas. However, around the globe, the empirical coefficients of the Hottel model have been provided for detailed values, corresponding to climate types. Therefore, under application conditions, the Hottel model can be used in areas with insufficient meteorological data.

The shadow of steel structures under sunlight directly affects the direct solar radiation absorbed by the structure's surface, and the analysis of the shadow effect is one important step in ensuring the accuracy of the simulation of temperature fields. Nowadays, shadow analysis methods mainly include the ray-tracing algorithm and the hemi-cube method. The ray-tracing algorithm originated from computer graphics, which calculates the incident path of sunlight based on the solar altitude angle and azimuth angle in order to judge the intersecting part between the sunlight and the surface of the steel structure, while permanent shadow due to closed spaces, structural self-shadow due to geometry, and environmental shadow caused by surrounding terrain can be identified by the algorithm [106–108]. The hemi-cube method was originally used to calculate the angle coefficient, which is the percentage of radiation energy emitted form one surface to another [109]. In the finite element software, the calculated angle coefficients are used to judge the irradiation elements and shaded elements, so the dynamic boundary between the irradiation and the shadow parts of the structural surface can be obtained in real time [110,111].

Convective heat transfer, which follows Newton's law of cooling, refers to the heat transfer between a solid surface and a fluid when the fluid flows through the solid, and its formula is shown in Equation (11).

$$q_c = h_c(T_a - T) \tag{11}$$

where q_c is the convective heat flux (W/m^2), h_c is the convective heat transfer coefficient ($W/(m^2 \cdot {}^\circ C)$), and T_a and T are the atmospheric temperature (°C) and the structure surface temperature (°C), respectively.

At present, there is no unified formula for calculating the convective heat transfer coefficient. Generally, the expressions of the convective heat transfer coefficient include two parts: free convection and forced convection. The air movement caused by the temperature difference between structure surface and atmosphere results in free convection, while forced convection is mainly caused by wind; free convection can be ignored when the wind speed is great enough. However, according to the principle of heat transfer, the coefficient of convective heat transfer should have an exponential relationship with wind speed. Nevertheless, many experiments have shown that the linear relationship can also be consistent with the test results; thus, the linear relation is feasible to use in many cases. Some representative expressions of the convective heat transfer coefficient in the study of the temperature fields of building structures are listed in Table 1.

Table 1. Representative expressions of convective heat transfer coefficient.

Number	Expression	Considered Factors	Variables Description
1 [112]	$h_c = 5.7 + 3.8v$	Wind speed	h_c is convective heat transfer coefficient; $h_{c,t}$, $h_{c,b}$, $h_{c,w}$ are the convective heat transfer of the outside surfaces of the top deck, bottom slab and web; $h_{c,i}$ is the convective heat transfer of the inside surfaces; v is the wind speed; v_0 is the wind speed under standard conditions; T_a, T are the air temperature and structure surface temperature, respectively; ΔT is the temperature difference between the structure surface and air; RE_L is Reynolds number; L is considered to be the longest dimension size of the panel element as a worst-case condition for convective heat transfer; ρ is the density of air; μ is the absolute viscosity of air; PR is Prandtl number; k is the heat con ductivity of air; C is a heat flow constant, and its value is related to the temperature difference between structure surface and air; T_{avg} is the average air film temperature, and can be approximated by the average of T and T_a
2 [113]	$h_c = (2.5 \sim 6.0) + 4.2v$	Wind speed	
3 [114]	$h_c = 5.6 + 4.0v$ for $v \le 5$ m/s $h_c = 7.2v^{0.78}$ for $v > 5$ m/s	Wind speed	
4 [115]	$h_c = 6.31v^{0.656} + 3.25e^{-1.91v}$ $h_c = 4.35 + 3.0v$ for $v \le 5$ m/s	Wind speed	
5 [104]	$h_{c,t} = 4.67 + 3.83v$ $h_{c,b} = 2.17 + 3.83v$ $h_{c,w} = 3.67 + 3.83v$ $h_{c,i} = 3.5$	Different parts of box girder, wind speed	
6 [101]	$h_c = 2.6\sqrt[4]{\lvert T_a - T\rvert} + 4.0v$	Temperature difference between the structure surface and air, wind speed	
7 [95]	Windward: $h_c = \sqrt{(0.84\Delta T^{1/3})^2 + (2.38{v_0}^{0.89})^2}$ Leeward: $h_c = \sqrt{(0.84\Delta T^{1/3})^2 + (2.86{v_0}^{0.617})^2}$	Windward and leeward, Temperature difference between the structure surface and air, wind speed	
8 [92]	For a flat surface of total length L, Laminar flow: $h_c = 0.664(RE_L)^{1/2}PR^{1/3}k/L$ turbulent flow: $h_c = 0.036(RE_L)^{1/1.25}PR^{1/3}k/L$ $RE_L = vL\rho/\mu$	Fluid state, wind speed	
9 [116]	$h_c = C \times 0.2782 \times \left[\frac{1}{T_{avg}+17.8}\right]^{0.181} \times$ $\lvert T - T_a\rvert^{0.266} \times \sqrt{1 + 2.8566v}$	Average temperature and temperature difference between the structure surface and air, wind speed	

3.2. Experimental Test

Compared with numerical simulations, experimental results are able to more accurately reflect the practical distribution and variation of the temperature fields and effects of steel structures.

Common temperature test equipment includes infrared radiation thermometers [117], thermal resistance sensors [23] and thermocouple sensor [29]. The measurement accuracy of infrared radiation thermometers is relatively low, so thermal resistance sensors and thermocouple sensors are mainly used in temperature field tests for steel structures.

Chen's experiment showed that the temperature of a single steel member along the length direction was relatively uniform, and the temperature difference along the thickness direction was negligible, but the temperature distribution through the cross-section was significantly non-uniform [22]. Therefore, temperature sensors are usually arranged along the mid-span section of a single steel member, as was adopted in the experiments of Wang [21] and Liu [20,118]. Space structures are composed of many steel members, and it is not realistic to monitor the temperatures of all of the members; only a few representative steel members are selected for temperature monitoring, and the selection of these representative members depends on the purpose of the measurements. To study the temperature characteristics of steel members under transparent and non-transparent roofs, Liu arranged the measurement areas under glass and light steel roofs, respectively, in the test scheme for the temperature field of the indoor water recreation project Tien Rice Cube [29]. Meanwhile, to further study the differences in temperature characteristics between the different types of steel members, Liu selected the top chord member, the bottom chord member, and a web member for temperature monitoring in the measurement areas, and four temperature sensors were set up along the mid-span section of each monitored member in order to measure their non-uniform temperature distributions. The temperature field test scheme of the Tien Rice Cube is shown in Figure 3. The conch-shaped single-layer steel lattice structure of the Yujiabu Railway Station Building is covered by ETFE membrane and glass; Zhao selected 11 steel members from the steel structure for temperature testing [119], and these members are shown in Figure 4. In order to analyze the differences in temperature characteristics between the members under the glass roof and the ETFE membrane, members 1, 2, 3, 5 and 11 were set under the glass roof, and the other 7 members were arranged under the ETFE membrane. In addition, the steel lattice structure can be divided into three parts: upper girder, upper lattice shell, and bottom girder; members 2 and 5 were located in the upper girder, member 11 was located in the bottom girder, and the other 8 members were located in the upper lattice shell. Similarly, four temperature sensors were arranged along the mid-span sections of each of the monitored rectangular or circular members.

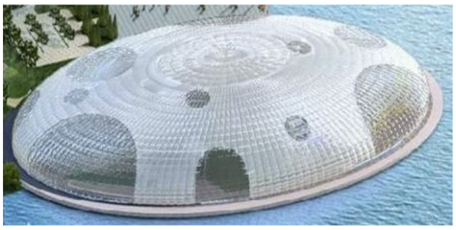

(**a**) Architectural effect Illustration

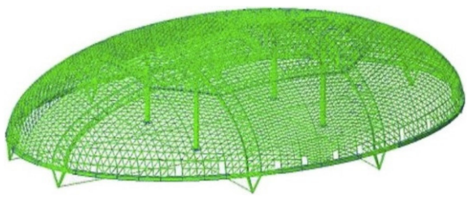

(**b**) Axonometric view

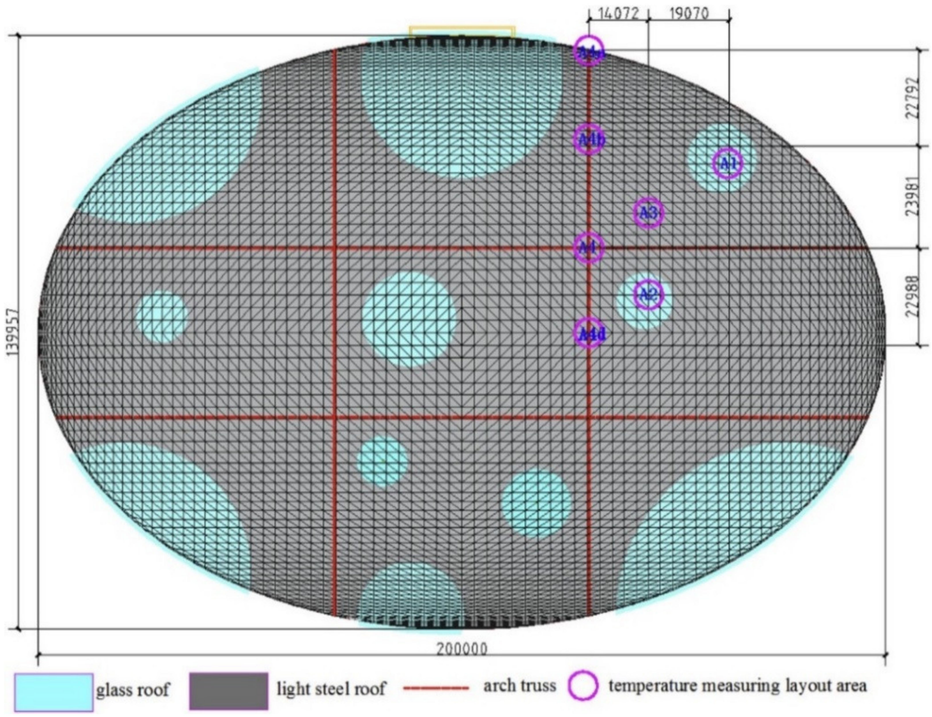

(**c**) Layout of temperature measurement areas

Figure 3. *Cont.*

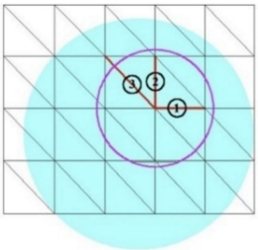

(**d**) Measurement area 1

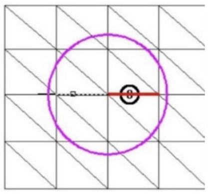

(**e**) Measurement area 3

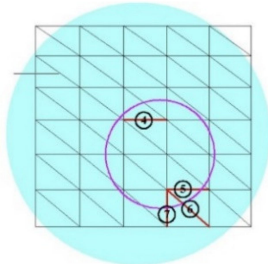

(**f**) Measurement area 2

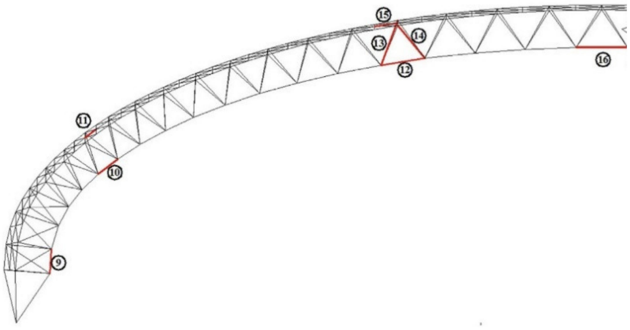

(**g**) Measurement area 4

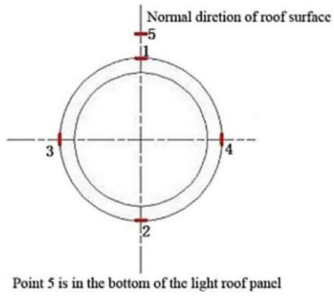

(**h**) Sensors for each member

Figure 3. Temperature field test scheme of the Tien Rice Cube (structural diagram, measuring point layout) [29].

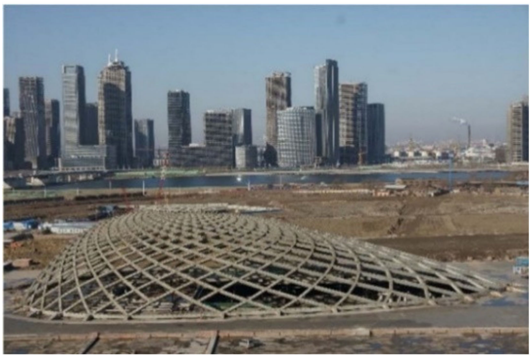

(**a**) Single-layer steel lattice structure

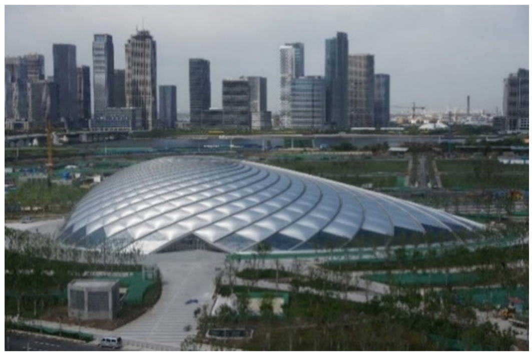

(**b**) Installed roof

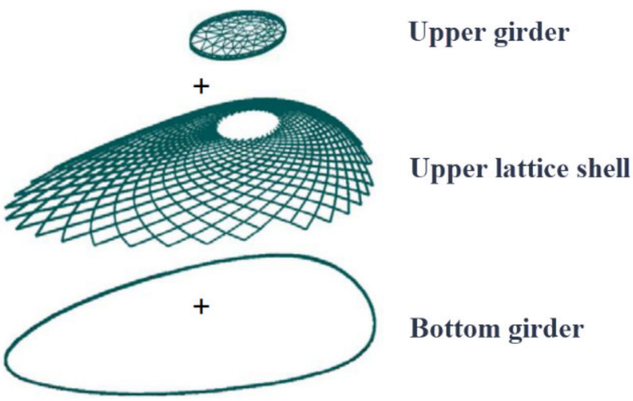

(**c**) Different components of the steel lattice structure

Figure 4. *Cont.*

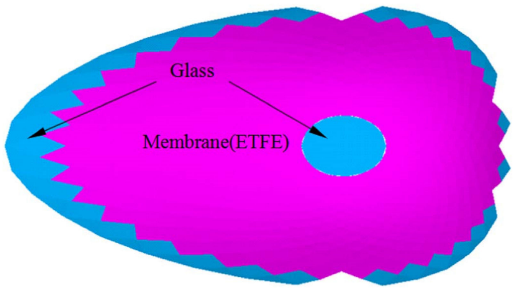

(**d**) Location of ETFE membrane and glass

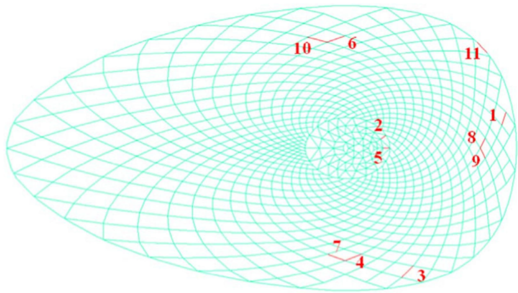

(**e**) Specific position of monitored members

(**f**) Measuring points of rectangular member

(**g**) Measuring points of circular member

Figure 4. Temperature field test scheme of the Yujiabu Railway Station Building (structural diagram, measuring point layout) [119].

The temperature field testing of bridges is usually carried out through the health monitoring system [120]; for example, 250 temperature sensors were installed in the six sections of the Confederation Bridge in order to monitor its real-time temperature field at hourly intervals [121]. In steel truss bridges, the layout of temperature sensors is similar to in space structures, and a limited number of steel trusses will be monitored according to the research objective. The Dashengguan Yangtze River Bridge and the Tongling Yangtze River Bridge are two typical steel truss bridges, the monitored members of which belong to the same cross-section in the longitudinal direction of the bridge in order to study the temperature difference between truss members, and several temperature sensors are also arranged in the mid-span section of the same truss member to study the temperature gradient of the truss section [43,44]; temperature tests of some other steel truss bridges also use this method for the layout of their temperature sensors [45]. Steel box girders in the bridge can be regarded as slender steel members, and the temperature gradient along the longitudinal direction is relatively small and can be ignored, which has been verified by previous studies [51,122]. Table 2 gives five temperature field test cases for steel box girders. In most test cases, only one section was arranged with temperature measuring points, and the temperature difference along the longitudinal direction of the steel box girder was ignored. Although four sections were selected at which to set measuring points in the test case of Runyang Bridge's steel box girder, the test data of Section III was mainly used for analyzing temperature field characteristics, and the temperature difference between sections were relatively small. All test results show that the temperature distribution of the cross-section is significantly non-uniform, and this non-uniformity was reflected in the vertical and horizontal temperature differences. Therefore, it is suggested that only one section be selected for temperature field monitoring, while the number of temperature sensors should be as large as possible in order to fully reflect the non-uniformity of the cross-section temperature field. In the daily state, the stay cables of cable-stayed bridges are in protection sleeves, and temperature monitoring is difficult to realize with conventional temperature sensors. In the temperature monitoring system of the Tsing Ma Bridge [60,61], several temperature sensors were embedded in the steel strands of the cables, and the effective temperature of a cable was taken as the average value of the temperatures monitored by these sensors; the specific locations of the embedded temperature sensors in the cable are shown in Figure 5.

Table 2. Five temperature field test cases for steel box girders.

Bridge	Number of Test Sections	Number of Measuring Points	Test Time	Test Area
Incheon Bridge [123]	1	7	June, from September to November, 2008	Incheon, South Korea
Layout of measuring points at the cross-section				

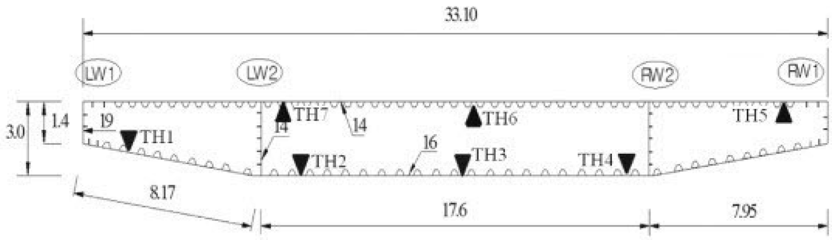

Bridge	Number of Test Sections	Number of Measuring Points	Test Time	Test Area
Sutong Bridge [124]	1	8	From January to December, 2011	Jiangsu, China
Layout of measuring points at the cross-section				

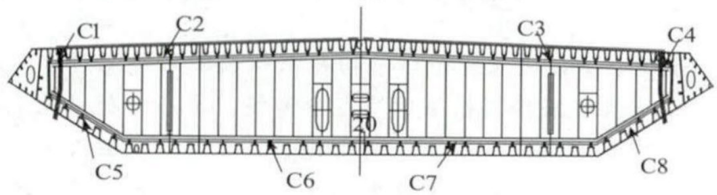

Bridge	Number of Test Sections	Number of Measuring Points	Test Time	Test Area
Nanxi Yangtze River Bridge [125]	1	15	From August 1 to December 1, 2014	Sichuan, China
Layout of measuring points at the cross-section				

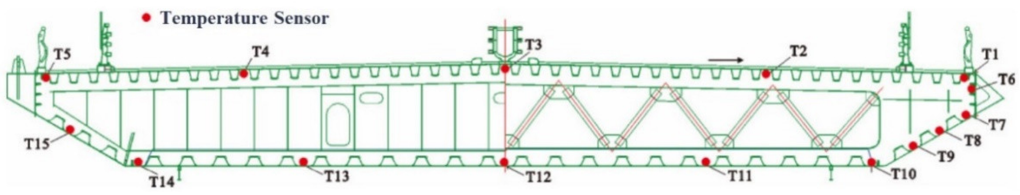

Bridge	Number of Test Sections	Number of Measuring Points	Test Time	Test Area
Normandy Bridge [51,52]	1	12	From February, 1996 to December, 1998	Normandy, France
Layout of measuring points at the cross-section				

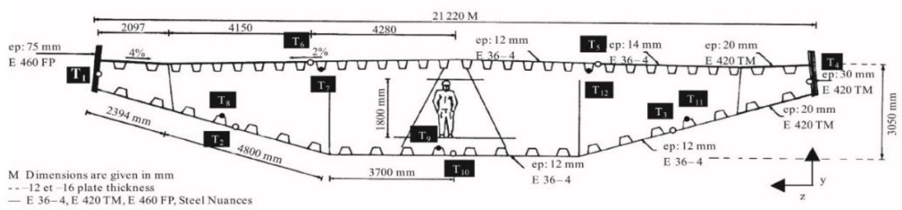

Bridge	Number of Test Sections	Number of Measuring Points	Test Time	Test Area
Runyang Bridge [57,126]	4	4 × 8	From 2005 to 2010	Jiangsu, China
Layout of measuring points at the cross-section				

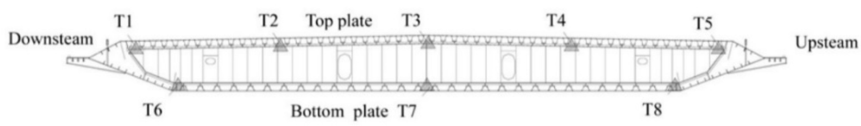

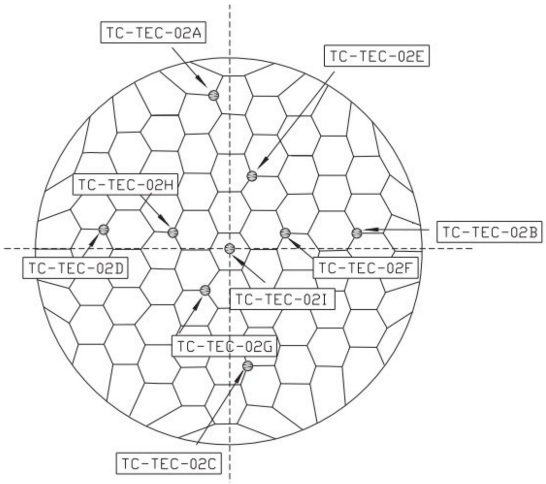

Figure 5. Embedded temperature sensors in the cable (cross-section view) [60,61].

A radio telescope is a type of large and complex steel structure, and a large number of temperature sensors are usually needed to measure its temperature field. Some cases of temperature field measurement for radio telescopes are shown in Table 3. As can be seen from the table, the number of temperature sensors exceeds 100 in most test cases. The layout of a large number of measuring points needs a corresponding strategy, which will be dependent on the purpose of the test and the intended use of the data. A general layout strategy is to arrange the temperature sensors uniformly according to the mass, volume and surface area of the telescope's structure, whereby 89 temperature sensors were arranged throughout the VertexRSI 12-m prototype telescope. The sensors on the fork support and backup structure were respectively determined on the basis of their approximately equal surface areas and volume [127]. Figure 6a gives the temperature measuring points layout of the VertexRSI 12-m prototype telescope. Bremer proposed one method for selecting the installation positions of the temperature sensors based on finite element analysis; specifically, the installation positions are the thermally important FE nodes, those which are able to produce the largest thermal deformation under a given temperature variation [128]. These two methods are the most commonly used at present. For the IRAM 30-m Telescope, the measuring points of the backup structure were arranged with uniform distribution according to volume, with the selection of the temperature sensors in the yoke being carried out on the basis of Bremer's method [129]. The layout of temperature measuring points for the IRAM 30-m Telescope is shown in Figure 6b.

Table 3. Some cases of temperature field tests for radio telescopes.

Radio Telescope	Reflector Diameter (m)	Measured Component	Number of Sensors
BIMA [79]	6	BUS	32
ASTE [130]	10	BUS, Pedestal, Fork	170
OVRO [79]	10.4	BUS	48
VertexRSI-ALMA [127]	12	Pedestal, Fork, BUS	89
AEC-ALMA [127]	12	Pedestal, Fork	101
ALMA-J [131]	12	BUS	227
FCRAO [132]	14	BUS, Quadripod, Subreflector	30
JCMT [79]	15	BUS, Alidade	220
IRAM [129]	30	Yoke, BUS, Quadripod	156
NRO [88,89]	45	BUS	140
RT-70 [133]	70	BUS	200

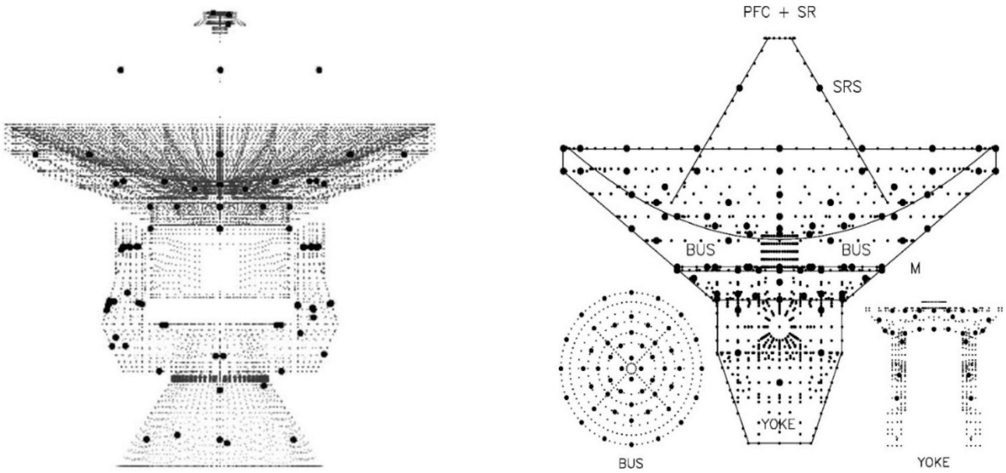

(**a**) (**b**)

Figure 6. Temperature measuring points layout of two radio telescope [127,129]. (**a**) VertexRSI 12-m prototype telescope. (**b**) IRAM 30-m Telescope.

The test contents when testing temperature effect include stress, displacement, cable force, etc.; stress can be measured by strain gauges [27] or vibrating wire sensors [30], displacement can be obtained using displacement transducers [60], GPS receivers [61] or 3D laser scanning [32], and cable force can be directly monitored by tension sensors [23] or calculated from displacement [63].

Generally, the measured temperature effect is used to analyze its relationship with the measured temperature, so the measurement point layout of the temperature effect is roughly consistent with that of temperature in many cases. Luo used 268 vibrating wire sensors, which integrate the test functions of stress and temperature, to measure the temperature and stress of the Beijing National Stadium's space truss structure in order to directly study the correlation between temperature field and stress, and the test results showed that the variation of temperature field was an important factor leading to high stress [30]. To study the relationship between the temperature field and the deflection of the steel box girder in the Zhijiang Cable-Stayed Bridge, 14 temperature sensors and 18 deflection sensors were arranged along the longitudinal direction of the bridge, with the longitudinal positions of T1-T14 and D3-D16 being the same [134]; the specific positions of these temperature and deflection sensors are shown in Figure 7. Based on comparative analysis of the test data, it was shown that the time-variance laws of girder temperature and girder deflection were similar, and there was a basically linear relationship between the temperature field and the deflection of the box girder at night, indicating that the girder deflection was greatly affected by the girder temperature. This method of determining the layout of measuring points to measure temperature effect was also applied in the studies of Chen [25], Zhao [27], Wang [45], etc.

In addition, measuring points are also arranged specifically at locations with significant temperature effects. Figure 8 shows the distribution of temperature sensors, strain gauges, GPS receivers and displacement transducers for the Tsing Ma Bridge [61]. From the figure, it can be seen that there are many differences in the arrangement of measuring points of temperature and temperature effect; the installed temperature sensors are concentrated in four areas for monitoring cable temperature and deck temperature, while the arrangement of temperature effect measuring points is much more intensive. The displacement measuring points (GPS receiver and displacement transducer) are not only arranged along the longitudinal direction to measure the overall displacement variation of the bridge, they are also placed in the bridge tower and main cable to monitor their movement, and the 110 strain gauges were installed in three deck sections to monitor for potentially large strain.

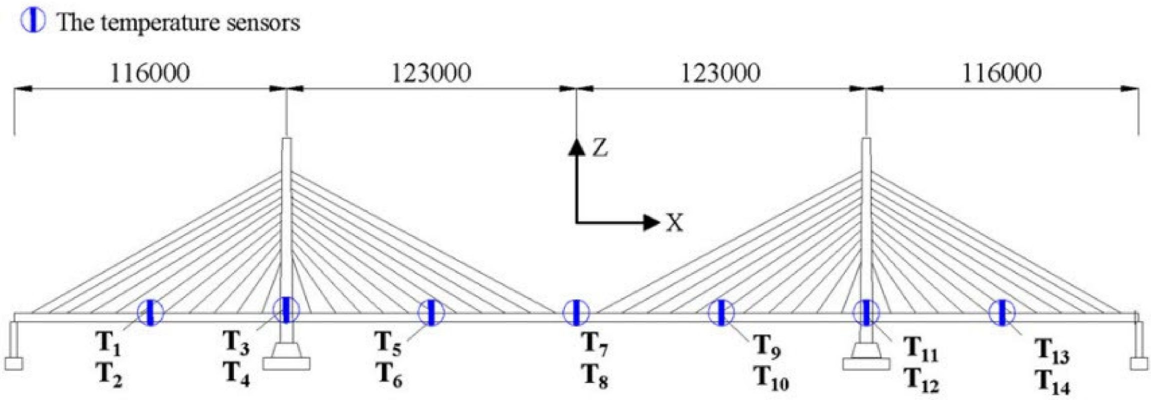

(**a**) Temperature sensors T1-T14

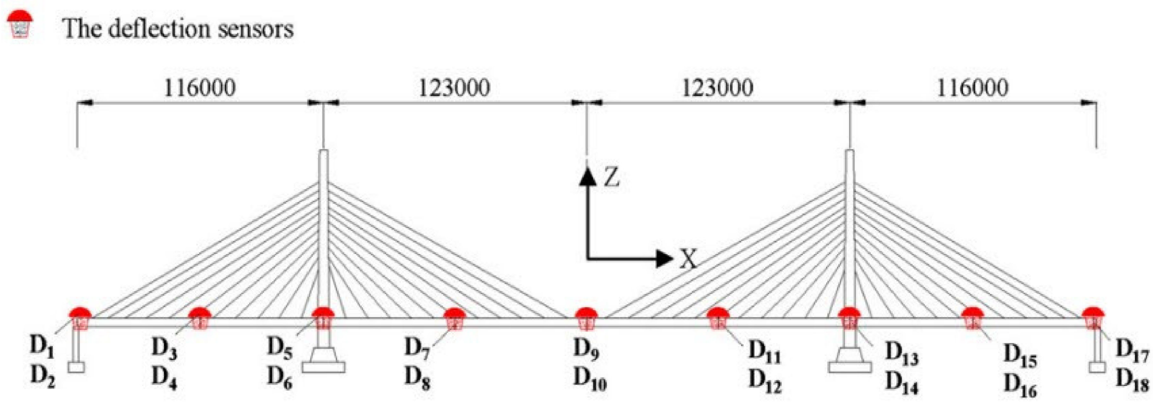

(**b**) Deflection sensors D1-D18

Figure 7. Locations of temperature and deflection sensors in the Zhijiang Cable-Stayed Bridge [134].

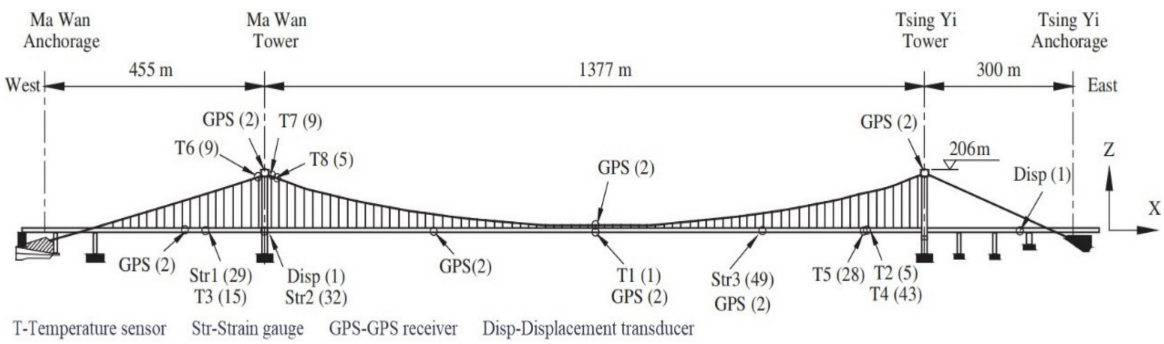

Figure 8. Distribution of temperature sensors, strain gauges, GPS receivers and displacement transducers in the Tsing Ma Bridge [61].

4. Outlook

The future of research on non-uniform temperature fields and effects in steel structures is exciting. Previous research results have been applied to the thermal design, thermal control, and thermal monitoring of steel structures, but some improvement and developments are also necessary.

4.1. Accurate Simulation of Temperature Field

The relationships among different factors involved in the simulation of the temperature fields of steel structures are shown in Figure 9. Too many simplifications and approximate values may lead to a great decrease in the accuracy of the temperature field simulation.

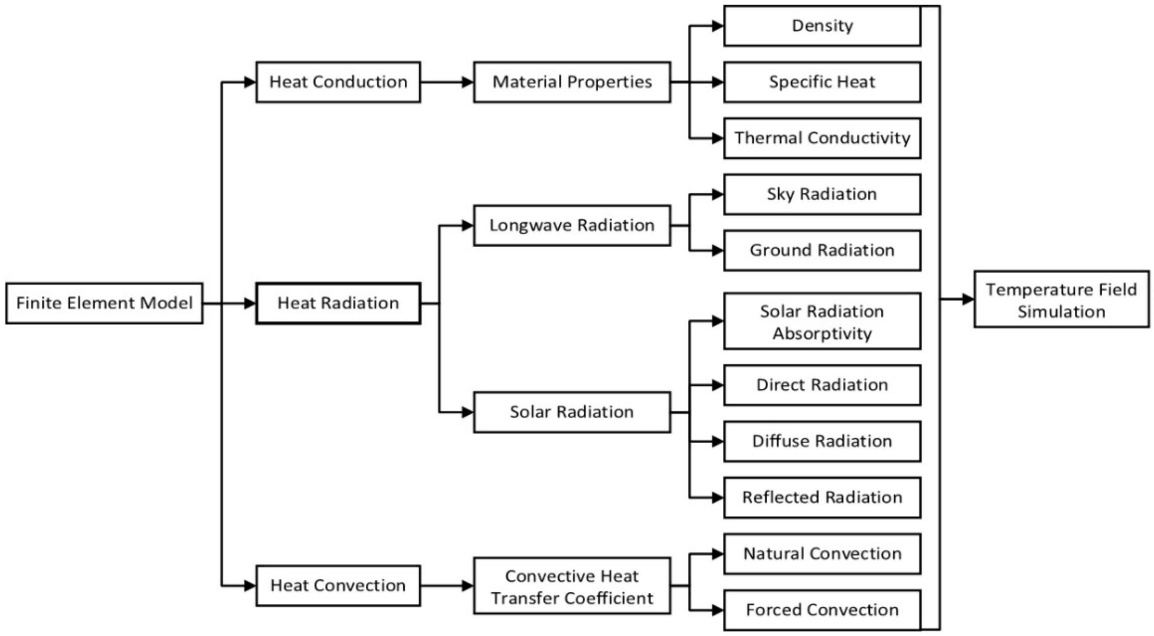

Figure 9. Flow chart of temperature field simulation of steel structures.

Solar radiation absorptivity reflects the ability of a steel structure to absorb solar radiation energy [135], which is related to the structure surface coating's color, chemical composition, roughness, etc. Due to the lack of sufficient test data, solar radiation absorptivity is usually approximately determined on the basis of the color of the coating on the surface of the steel structure [37,136]. However, even for different coatings of the same color, the difference in solar radiation absorptivity can be up to 67% [117]. The temperature fields of steel structures are very sensitive to solar radiation [137], and the accuracy of the temperature field simulation may be greatly reduced by adopting approximate value methods for solar radiation absorptivity. Therefore, a large number of solar radiation absorptivity tests should be carried out, according to the categories of steel structure surface coatings, and a detailed database needs to be established, which will not only be helpful for the thermal research of civil engineering, but will also be beneficial in aerospace engineering, vehicle engineering, environmental science, etc.

There are many thermal boundary conditions, such as air temperature, wind speed and solar radiation intensity, that affect the temperature field of steel structures, and accurate thermal boundary conditions are key to ensuring the accuracy of temperature field simulations. In many studies, thermal boundary conditions have been calculated using simplified formulas, but these calculation results may differ greatly from the real thermal boundary conditions, whose variations are complex and difficult to accurately predict. Therefore, it is recommended that thermal boundary conditions obtained from a meteorological department or the measured data be used [138]. The long-term temperature field of steel structure can be simulated with multi-year meteorological data as the input for thermal boundary conditions, and this can be used as a basis for studying extreme temperature events and time-variance of temperature fields, which will provide opportunities for improving structural design methods and perfecting design specifications.

4.2. Improvement of Test Method

The temperature field of steel structures cannot be fully obtained based on the test data from a limited number of temperature measurement points, and the temperature gradient in local areas is also difficult to accurately measure. Infrared thermal imaging detects the infrared band signal of the object's thermal radiation through photoelectric technology, and the signal is converted into an image that effectively reflects the distribution of the temperature field for visual discrimination [139,140]. Imaging technology has been widely used in medicine [141–143], the military [144–146], industry [147–149], agriculture [150–152], and architecture [153–155], but it is rarely used in the measurement of the temperature field of steel structures. A reasonable arrangement of a sufficient number of high-precision thermal imagers can accurately obtain the actual distribution of the temperature field of a steel structure; meanwhile, in combination with the shadow variation captured by an HD camera, the distribution mechanism and time-variance laws of the temperature field of a steel structure can be deeply understood. Figure 10 shows a photo and a thermal image of the Hong Kong-Zhuhai-Macao Bridge.

(**a**) photo

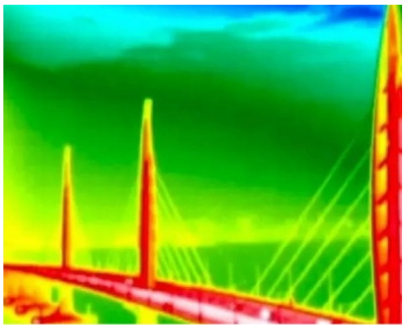

(**b**) thermal image

Figure 10. Photo and thermal image of the Hong Kong-Zhuhai-Macao Bridge.

The measured effect of a steel structure is a result of the combined action of temperature load, wind load, and other loads, such as vehicle and train loads, and it is difficult to completely remove the influences of other loads to obtain the temperature effect directly, which leads to differences between test results and the practical temperature effect. In addition, test equipment, such as strain gauges, expand and contract with temperature variations during the test process, which may further affect the accuracy when evaluating temperature effect. Excluding the influence of other factors and directly obtaining the accurate temperature effect of steel structures is currently a difficult research problem, and will also be the focus of future research.

4.3. Other Aspects

One important purpose of research into the non-uniform temperature fields and effects of steel structures is to improve existing design methods. Research into the non-uniform temperature distribution mechanism and the time-variance laws of bridge structures is relatively mature, and on this basis, many bridge codes provide systematic and detailed theories and methods with respect to non-uniform temperature design [156–158]. However, for other complex steel structures, such as space structures and radio telescopes, there are no systematic design methods for non-uniform temperatures; thus, they should be a research focus in this field in order to establish simplified and feasible design methods for the non-uniform temperature loads of these structures at the next stage.

Many studies [36,73,134] have shown that non-uniform temperature-induced effects have a significant adverse effect on the performance of steel structures, but few studies have referred to a method for reducing these adverse effects. The application of radiation-proof paint effectively reduces the ability of steel structures to absorb solar radiation energy, or enhance the convective effect by strengthening the air flow at the steel structure's surface, then lowering the structural temperature and weakening the temperature effect. In addition, the design of stress relief devices, such as sliding bearing, based on non-uniform temperature loads is also an effective method for counteracting the effects of thermal expansion and contraction, and weakening the temperature effect. The above two ideas are available for research, and the specific methods can be established through future careful analysis and testing.

Global warming is becoming more and more serious with the intensification of the greenhouse effect, as has been reflected in many studies [159–161]. Based on the report of the World Meteorological Organization [162], the five-year period 2015–2019 is the warmest of any equivalent period on record globally, and extremely high temperatures have appeared in many regions, with two major heatwaves being recorded in Europe in June-July 2019, and national records being broken in many countries. The temperature rise caused by global warming will directly affect the temperature fields of steel structures, leading to more significant thermal effects. The effect of global warming on climate cannot be ignored during the design period of steel structures, but the global warming effect has not been considered in previous studies on the temperature fields and effects of steel structures [163]. As one research direction in the future, a study on the influence of global warming on steel structure temperatures would be of practical value.

5. Conclusions

In this paper, previous studies on non-uniform temperature fields and effects in steel structures are summarized, temperature field simulation principles are described based on the heat transfer mechanism, and experimental test methods for temperature and effect are introduced through the analysis of typical test cases. Based on research into space structures, bridges and radio telescopes, the temperature field of steel structures can be seen to be significantly non-uniform, and the temperature-induced effect can not only directly affect the structural working performance, but can also induce some potential safety hazards. Currently, the numerical simulation of temperature field is relatively mature, and many scholars have improved the simulation method through their studies, including the establishment of solar radiation calculation models, shadow analysis algorithms, and convective heat transfer coefficient expressions. In different test cases, the researchers have formulated corresponding test schemes according to their research object and content: the sensors of slender members are usually arranged along the cross-section, and test points are only set at representative members for large complex structures, according to the research object. Based on the above summary, some suggestions of development and improvement for studies in this field are given. In the test methods, some difficult problems need to be solved, and the application of new test techniques and equipment is suggested. To improve the simulation accuracy of temperature fields, the solar radiation absorptivity for different coatings should be accurately tested using a large number of tests, and the practical thermal conditions need to be obtained from meteorological departments or on-site measurement. In addition, other aspects are also worth studying and exploring, for example, the establishment of general design methods for non-uniform temperature loads, solutions to the adverse effects of non-uniform temperature effects and the influence of global warming on steel structure temperature.

Author Contributions: Conceptualization, W.X. and D.C.; methodology, W.X.; formal analysis, W.X.; investigation, W.X.; writing—original draft, W.X.; writing—review and editing, W.X. and D.C.; resources, D.C.; funding acquisition, D.C.; project administration, H.Q. All authors have read and agreed to the published version of the manuscript.

Funding: This study was supported by the National Natural Science Foundation of China (Grant No. 51808168), the China Postdoctoral Science Foundation (Grant No. 2020M672132) and the Fundamental Research Funds for the Central Universities (Grant No.HIT.NSRIF.2019079).

Conflicts of Interest: The authors declare that they have no conflict of interest.

References

1. Yu, Y.Q.; Zhu, F.Q.; Wang, Z. Review of the Promotion and Application of Steel Structures in Construction. *Steel Constr.* **2020**, *35*, 59–69.
2. Liu, H.B.; Chen, Z.H.; Zhou, T. Investigation on temperature distribution and thermal behavior of large span structures considering solar radiation. *Adv. Steel Constr.* **2013**, *9*, 41–58.

3. Chen, D.S.; Qian, H.L.; Wang, H.J.; Xu, W.C.; Li, J.F. Non-Uniform Temperature Field of Spatial Grid Structure under Construction Induced by Solar Radiation. *Appl. Sci.* **2020**, *10*, 2445. [CrossRef]
4. Ministry of Housing and Urban-Rural Development of the People's Republic of China. *Load Code for the Design of Building Structures*; GB50009-2012; China Architectural & Building Press: Beijing, China, 2012.
5. Ministry of Housing and Urban-Rural Development of the People's Republic of China. *Code for Design of Steel Structures*; GB50017-2003; China Architectural & Building Press: Beijing, China, 2003.
6. Ministry of Housing and Urban-Rural Development of the People's Republic of China. *Technical Specification for Space Frame Structures*; JGJ7-2010; China Architectural & Building Press: Beijing, China, 2010.
7. Fan, Z. Key Techniques of Large-span Structure Design for Beijing National Stadium. *J. Build. Struct.* **2006**, *36*, 34–43.
8. Chen, D.S.; Xu, W.C.; Qian, H.L.; Sun, J.Y.; Li, J.F. Effects of non-uniform temperature on closure construction of spatial truss structure. *J. Build. Eng.* **2020**, *32*, 101532. [CrossRef]
9. Liu, H.B.; Chen, Z.H. *Non-Uniform Temperature Effect of Large-Span Building Structure Considering Solar Radiation*; Science Press: Beijing, China, 2016.
10. Liu, H.B.; Zhang, Z.S.; Chen, Z.H.; Chen, Q. Research on temperature field and temperature effect of steel silos under solar radiation. *J. Build. Struct.* **2016**, *37*, 151–157.
11. Liu, H.B.; Ying, J.J.; Chen, Z.Z. Study overviews of non-uniform thermal behavior of spatial structures under solar radiation. *Build. Struct.* **2017**, *47*, 59–63.
12. Song, Y.S.; Ding, Y.L. Fatigue monitoring and analysis of orthotropic steel deck considering traffic volume and ambient temperature. *Sci. China Technol. Sci.* **2013**, *56*, 1758–1766. [CrossRef]
13. Xia, Y.; Chen, B.; Wen, S.; Ni, Y.Q.; Xu, Y.L. Temperature effect on vibration properties of civil structures: A literature review and case studies. *J. Civ. Struct. Health Monit.* **2012**, *2*, 29–46. [CrossRef]
14. Schindler, A.K.; Hughes, M.L.; Barnes, R.W.; Byard, B.E. Evaluation of cracking of the US 331 bridge deck. In *Research Report, Highway Research Center, 238 Harbert Engineering Center*; Auburn University: Auburn, AL, USA, 2010.
15. Jin, X.F. Study of Key Issues of the Structural Safety and Accuracy Control of the Five-Hundred-Meter Aperture Radio Telescope. Ph.D. Thesis, Harbin Institute of Technology, Harbin, China, 2010.
16. Alinia, M.M.; Kashizadeh, S. Effects of support positioning on thermal behaviour of double layer space truss domes. *J. Constr. Steel Res.* **2007**, *63*, 375–382. [CrossRef]
17. Alinia, M.M.; Kashizadeh, S. Effect of flexibility of substructures upon thermal behaviour of spherical double layer space truss domes. Part I: Uniform thermal loading. *J. Constr. Steel Res.* **2006**, *62*, 359–368. [CrossRef]
18. Alinia, M.M.; Kashizadeh, S. Effect of flexibility of substructures upon thermal behaviour of spherical double layer space truss domes. Part II: Gradient & partial loading. *J. Constr. Steel Res.* **2006**, *62*, 675–681. [CrossRef]
19. Liu, H.B. Study on the Construction Control Theory and Temperature Effect of Suspen-Dome Structure. Ph.D. Thesis, Tianjin University, Tianjin, China, 2011.
20. Liu, H.B.; Chen, Z.H.; Zhou, T. Numerical and experimental investigation on the temperature distribution of steel tubes under solar radiation. *Struct. Eng. Mech.* **2012**, *43*, 725–737. [CrossRef]
21. Wang, Y.Q.; Lin, C.C.; Shi, Y.J. Experimental study on the temperature of steel members in sunshine. *J. Build. Struct.* **2010**, *31*, 140–147.
22. Chen, D.S.; Qian, H.L.; Wang, H.J.; Chen, Y.; Fan, F.; Shen, S.Z. Experimental and numerical investigation on the non-uniform temperature distribution of thin-walled steel members under solar radiation. *Thin Walled Struct.* **2018**, *122*, 242–251. [CrossRef]
23. Chen, D.S. Experimental and Numerical Investigation of the Non-Uniform Temperature Field and the Effect on Spatial Steel Structures under Solar Radiation. Ph.D. Thesis, Harbin Institute of Technology, Harbin, China, 2017.
24. Liu, H.B.; Chen, Z.H.; Chen, B.B.; Xiao, X.; Wang, X.D. Studies on the temperature distribution of steel plates with different paints under solar radiation. *Appl. Therm. Eng.* **2014**, *71*, 342–354. [CrossRef]
25. Chen, D.S.; Wang, H.J.; Qian, H.L.; Li, X.Y.; Fan, F.; Shen, S.Z. Experimental and numerical investigation of temperature effects on steel members due to solar radiation. *Appl. Therm. Eng.* **2017**, *127*, 696–704. [CrossRef]
26. Zhao, Z.W. Researches on Erection Simulation Optimization and Thermal Effect of Large-Span Double-Helix Single-Layer Latticed Shell Structure. Ph.D. Thesis, Tianjin University, Tianjin, China, 2016.
27. Zhao, Z.W.; Liu, H.B.; Chen, Z.H. Field monitoring and numerical analysis of thermal behavior of large span steel structures under solar radiation. *Adv. Steel Constr.* **2017**, *13*, 190–205.

28. Liu, H.B.; Li, B.; Chen, Z.H.; Zhou, T.; Zhang, Q. Solar radiation properties of common membrane roofs used in building structures. *Mater. Des.* **2016**, *105*, 268–277. [CrossRef]
29. Liu, H.B.; Liao, X.W.; Chen, Z.H.; Zhang, Q. Thermal behavior of spatial structures under solar irradiation. *Appl. Therm. Eng.* **2015**, *87*, 328–335. [CrossRef]
30. Luo, Y.Z.; Mei, Y.J.; Shen, Y.B.; Yang, P.C.; Jin, L.; Zhang, P.F. Field measurement of temperature and stress on steel structure of the National Stadium and analysis of temperature action. *J. Build. Struct.* **2013**, *34*, 24–32.
31. Pei, Y.; Bai, Y.; Shi, Y.; Zhu, D.; Wang, Y. Temperature distribution in a long-span aircraft hangar. *Tsinghua Sci. Technol.* **2008**, *13*, 184–190. [CrossRef]
32. Zhou, M.; Fan, J.S.; Liu, Y.F.; Zhang, J.X.; Duan, X.J.; Lei, S.S. Non-uniform temperature field and effect on construction of large-span steel structures. *Autom. Constr.* **2020**, *119*, 103339. [CrossRef]
33. Liu, H.B.; Chen, Z.H.; Zhou, T. Temperature distribution and structural behavior of box-sectional arch structures under solar radiation. *Adv. Steel Constr.* **2013**, *9*, 298–308. [CrossRef]
34. Liu, H.B.; Chen, Z.H.; Han, Q.H.; Chen, B.B.; Bu, Y.D. Study on the thermal behavior of aluminum reticulated shell structures considering solar radiation. *Thin Walled Struct.* **2014**, *85*, 15–24. [CrossRef]
35. Liu, H.B.; Chen, Z.H.; Zhou, T. Research on the Process of Pre-Stressing Construction of Suspen-Dome Considering Temperature Effect. *Adv. Struct. Eng.* **2012**, *15*, 489–493. [CrossRef]
36. Liu, H.B.; Chen, Z.H. Non-Uniform Thermal Behaviour of Suspen-Dome with Stacked Arch Structures. *Adv. Struct. Eng.* **2013**, *16*, 1001–1009. [CrossRef]
37. China Association for Engineering Construction Standardization. *Technical Specification for Retractable Roof Structures*; CECS 417:2015; China Planning Press: Beijing, China, 2015.
38. Ministry of Housing and Urban-Rural Development of the People's Republic of China. *Technical Standard for Retractable Roof Structures*; JGJ/T 442-2019; China Architectural & Building Press: Beijing, China, 2019.
39. Liu, Y.; Qian, Z.D.; Hu, H.Z. Thermal field characteristic analysis of steel bridge deck during high-temperature asphalt pavement paving. *KSCE J. Civ. Eng.* **2016**, *20*, 2811–2821. [CrossRef]
40. Wang, D.; Liu, Y.M.; Liu, Y. 3D temperature gradient effect on a steel-concrete composite deck in a suspension bridge with field monitoring data. *Struct. Control Health Monit.* **2018**, *25*, e2179. [CrossRef]
41. Liu, W.S.; Dai, G.L.; Rao, S.C. Numerical calculation on solar temperature field of a cable-stayed bridge with U-shaped section on high-speed railway. *J. Cent. South Univ.* **2014**, *21*, 3345–3352. [CrossRef]
42. Wang, J.F.; Zhang, J.T.; Xu, R.Q.; Yang, Z.X. Evaluation of Thermal Effects on Cable Forces of a Long-Span Prestressed Concrete Cable-Stayed Bridge. *J. Perform. Constr. Facil.* **2019**, *33*, 04019072. [CrossRef]
43. Wang, G.X.; Ding, Y.L.; Liu, X.W. The monitoring of temperature differences between steel truss members in long-span truss bridges compared with bridge design codes. *Adv. Struct. Eng.* **2019**, *22*, 1453–1466. [CrossRef]
44. Wang, G.X.; Ding, Y.L. Research on monitoring temperature difference from cross sections of steel truss arch girder of Dashengguan Yangtze Bridge. *Int. J. Steel Struct.* **2015**, *15*, 647–660. [CrossRef]
45. Wang, G.X.; Ding, Y.L.; Sun, P.; Wu, L.L.; Yue, Q. Assessing Static Performance of the Dashengguan Yangtze Bridge by Monitoring the Correlation between Temperature Field and Its Static Strains. *Math. Probl. Eng.* **2015**, *2015*, 12. [CrossRef]
46. State Railway Administration. *Code for Design on Railway Bridge and Culvert*; TB 10002-2017; China Railway Publishing House: Beijing, China, 2017.
47. Wang, G.X.; Ding, Y.L. Long-Term Monitoring of Temperature Effect on Horizontal Rotation Angle at Beam Ends of a Railway Steel Truss Bridge. *J. Bridge Eng.* **2019**, *24*, 05019012. [CrossRef]
48. Wang, G.X.; Ding, Y.L. Reliability Estimation of Horizontal Rotation at Beam End of Long-Span Continuous Truss Bridge Affected by Temperature Gradients. *J. Perform. Constr. Facil.* **2019**, *33*, 04019061. [CrossRef]
49. Ding, Y.L.; Zhou, G.D.; Li, A.Q.; Wang, G.X. Thermal Field Characteristic Analysis of Steel Box Girder Based on Long-term Measurement Data. *Int. J. Steel Struct.* **2012**, *12*, 219–232. [CrossRef]
50. European Committee for Standardization. *Eurocode 1: Actions on Structures-Part 1–5: General Actions-Thermal Actions*; BS EN 1991-1-5: 2003; European Committee for Standardization: Brussels, Belgium, 2003.
51. Lucas, J.M.; Virlogeux, M.; Louis, C. Temperature in the Box Girder of the Normandy Bridge. *Struct. Eng. Int.* **2005**, *15*, 156–165. [CrossRef]
52. Lucas, J.M.; Berred, A.; Louis, C. Thermal actions on a steel box girder bridge. *Proc. Inst. Civ. Eng. Struct. Build.* **2003**, *156*, 175–182. [CrossRef]

53. Tong, M.; Tham, L.G.; Au, F.T.K. Extreme thermal loading on steel bridges in tropical region. *J. Bridge Eng.* **2002**, *7*, 357–366. [CrossRef]
54. Au, F.T.K.; Tham, L.G.; Tong, M. Design thermal loading for steel bridges in Hong Kong. *HKIE Trans.* **2001**, *8*, 1–9. [CrossRef]
55. Miao, C.Q.; Shi, C.H. Temperature gradient and its effect on flat steel box girder of long-span suspension bridge. *Sci. China Technol. Sci.* **2013**, *56*, 1929–1939. [CrossRef]
56. Zhou, L.R.; Xia, Y.; Brownjohn, J.M.W.; Koo, K.Y. Temperature Analysis of a Long-Span Suspension Bridge Based on Field Monitoring and Numerical Simulation. *J. Bridge Eng.* **2016**, *21*, 04015027. [CrossRef]
57. Ding, Y.L.; Wang, G.X. Estimating extreme temperature differences in steel box girder using long-term measurement data. *J. Cent. South Univ.* **2013**, *20*, 2537–2545. [CrossRef]
58. Park, S.J.; Kim, Y.G.; Kim, S.H. A study on Temperature variation of Steel box girder for construction of Key-segment Closure of Partially Earth-anchored Cable-stayed Bridges. In Proceedings of the 6th International Conference on Bridge Maintenance, Safety and Management (IABMAS), Stresa, Italy, 8–12 July 2012; pp. 3638–3642.
59. Wang, J.F.; Xu, Z.Y.; Fan, X.L.; Lin, J.P. Thermal Effects on Curved Steel Box Girder Bridges and Their Countermeasures. *J. Perform. Constr. Facil.* **2017**, *31*, 04016091. [CrossRef]
60. Xia, Y.; Chen, B.; Zhou, X.Q.; Xu, Y.L. Field monitoring and numerical analysis of Tsing Ma Suspension Bridge temperature behavior. *Struct. Control Health Monit.* **2013**, *20*, 560–575. [CrossRef]
61. Xu, Y.L.; Chen, B.; Ng, C.L.; Wong, K.Y.; Chan, W.Y. Monitoring temperature effect on a long suspension bridge. *Struct. Control Health Monit.* **2010**, *17*, 632–653. [CrossRef]
62. Zhou, Y.; Sun, L.M. A comprehensive study of the thermal response of a long-span cable-stayed bridge: From monitoring phenomena to underlying mechanisms. *Mech. Syst. Signal Proc.* **2019**, *124*, 330–348. [CrossRef]
63. Yang, D.H.; Yi, T.H.; Li, H.N.; Zhang, Y.F. Monitoring and analysis of thermal effect on tower displacement in cable-stayed bridge. *Measurement* **2018**, *115*, 249–257. [CrossRef]
64. Zhang, G. Experimental Research on Sunshine Non-Uniform Temperature Field of Radio Telescope. Master's Thesis, Harbin Institute of Technology, Harbin, China, 2015.
65. Hessels, J. X marks the spot for fast radio bursts. *Nature* **2019**, *572*, 320–321. [CrossRef]
66. Ransom, S.M.; Hessels, J.W.T.; Stairs, I.H.; Freire, P.C.C.; Camilo, F.; Kaspi, V.M.; Kaplan, D.L. Twenty-one millisecond pulsars in Terzan 5 using the Green Bank Telescope. *Science* **2005**, *307*, 892–896. [CrossRef] [PubMed]
67. Greve, A.; Kaercher, H.J. Performance Improvement of a Flexible Telescope Through Metrology and Active Control. *Proc. IEEE* **2009**, *97*, 1412–1420. [CrossRef]
68. Qian, H.L.; Liu, Y.; Fan, F.; Fu, L.; Liu, G.X. Analysis of the Precision of the Structural Performance of the 5 m-Antenna Reflector. *Int. J. Space Struct.* **2013**, *28*, 15–26. [CrossRef]
69. Nan, R.D.; Li, D.; Jin, C.J.; Wang, Q.M.; Zhu, L.C.; Zhu, W.B.; Zhang, H.Y.; Yue, Y.L.; Qian, L. The Five-hundred-meter Aperture Spherical Radio Telescope (FAST) Project. *Int. J. Mod. Phys. D* **2011**, *20*, 989–1024. [CrossRef]
70. Kildal, P.S.; Baker, L.A.; Hagfors, T. The Arecibo Upgrading: Electrical Design and Expected Performance of the Dual-Reflector Feed System. *Proc. IEEE* **1994**, *82*, 714–724. [CrossRef]
71. Shen, S.Z.; Fan, F.; Qian, H.L. Research on support structure scheme for active reflector of FAST. *J. Build. Struct.* **2010**, *31*, 1–8.
72. Wang, Q.M.; Zhu, M.; Wang, Q.M.; Yang, L.; Lei, Z. The Monitoring of Temperature Effect on the Supporting Structure of Main Active Reflector for FAST. In Proceedings of the 2nd International Conference on Mechanics, Materials and Structural Engineering (ICMMSE), Beijing, China, 14–16 April 2017; pp. 201–207.
73. Fan, F.; Jin, X.F.; Shen, S.Z. Effect of Non-uniform Solar Temperature Field on Cable-net Structure of Reflector of Large Radio Telescope-FAST. *Adv. Struct. Eng.* **2009**, *12*, 503–512. [CrossRef]
74. Jin, X.F.; Fan, F.; Shen, S.Z. Effect of non-uniform temperature field under sunshine on the structure supporting the reflector of a large radio telescope-FAST. *China Civ. Eng. J.* **2008**, *41*, 71–77.
75. Liu, Y. Non-uniform Solar Temperature Field on Large Aperture, Fully-Steerable Telescope Structure. *J. Astrophys. Astron.* **2016**, *37*, 19. [CrossRef]
76. Greve, A.; MacLeod, G. Thermal model calculations of enclosures for millimeter wavelength radio telescopes. *Radio Sci.* **2001**, *36*, 1111–1128. [CrossRef]

77. Greve, A.; Bremer, M. Calculated thermal behavior of ventilated high precision radio telescopes. *IEEE Antennas Propag. Mag.* **2006**, *48*, 9–19. [CrossRef]
78. Bremer, M.; Greve, A. A dynamic thermal Model for Design and Control of an 800-Element Open-Air Radio Telescope. In Proceedings of the Conference on Integrated Modeling of Complex Optomechanical Systems, Kiruna, Sweden, 15–17 August 2011, 83360U.
79. Greve, A.; Bremer, M. *Thermal Design and Thermal Behavior of Radio Telescopes and Their Enclosures*; Springer: Berlin, Germany, 2010.
80. Qian, H.L.; Chen, D.S.; Fan, F.; Liu, Y.; Shen, S.Z. Evaluation of solar temperature field under different wind speeds for Shanghai 65 m radio telescope. *Int. J. Steel Struct.* **2016**, *16*, 383–393. [CrossRef]
81. Zhong, J.; Qian, H.L.; Fan, F.; Shen, S.Z. An estimate of the time-varying temperature field of the main reflector and subreflector of the Shanghai 65 m radio telescope under solar illumination. *Int. J. Steel Struct.* **2016**, *16*, 115–124. [CrossRef]
82. Fan, F. Mechanical analysis report on Shanghai 65 m radio telescope structure. In *Research Report, Space Structure Research Center of Harbin Institute of Technology*; Harbin Institute of Technology: Harbin, China, 2010.
83. Qian, H.L.; Liu, Y.; Fan, F.; Fu, L.; Liu, G.X. The Analysis of Solar Radiation of Shanghai 65 m Radio Telescope. *Eng. Mech.* **2012**, *29*, 378–384. [CrossRef]
84. Zhong, J. Research on Non-Uniform Temperature Field of Giant Radio Telescopes. Master's Thesis, Harbin Institute of Technology, Harbin, China, 2012.
85. Liu, G.X.; Zheng, Y.P. Report on design of Shanghai 65 m antenna structure. In *Research Report, The 54th Research Institute of China Electronics Technology Group Corporation*; China Electronics Technology Group: Shijiazhuang, China, 2009.
86. Borovkov, A.; Shevchenko, D.V.; Gimmelman, V.G.; Machuev, Y.I.; Gaev, A.V. Finite-element modeling and thermal analysis of the RT-70 radio telescope main reflector. In Proceedings of the 4th International Conference on Antenna Theory and Techniques, Sevastopol, Ukraine, 9–12 September 2003; pp. 651–654.
87. Prestage, R.M.; Constantikes, K.T.; Balser, D.S.; Condon, J.J. The GBT Precision Telescope Control System. In Proceedings of the Conference on Ground-Based Telescopes, Glasgow, UK, 21–25 June 2004; pp. 1029–1040.
88. Ukita, N. Thermal effects on the pointing of the Nobeyama 45-m telescope. *Publ. Natl. Astron. Obs. Jpn.* **1999**, *5*, 139–147.
89. Akabane, K. A large millimeter wave antenna. *Int. J. Infrared Millim. Waves* **1983**, *4*, 793–808. [CrossRef]
90. Nindos, A.; Kontar, E.P.; Oberoi, D. Solar physics with the Square Kilometre Array. *Adv. Space Res.* **2019**, *63*, 1404–1424. [CrossRef]
91. Corder, S.; Cox, P. Atacama large millimeter/submillimeter array: Progress, status, and development. In Proceedings of the Conference on Ground-Based and Airborne Telescopes V, Montreal, QC, Canada, 22–27 June 2014. 91451V.
92. Chen, D.S.; Qian, H.L.; Wang, H.J.; Zhang, G.; Fan, F.; Shen, S.Z. Non-uniform temperature field measurement and simulation of a radio telescope's main reflector under solar radiation. *Appl. Therm. Eng.* **2017**, *111*, 1330–1341. [CrossRef]
93. Chen, D.S.; Wang, H.J.; Qian, H.L.; Zhang, G.; Shen, S.Z. Solar cooker effect test and temperature field simulation of radio telescope subreflector. *Appl. Therm. Eng.* **2016**, *109*, 147–154. [CrossRef]
94. Qian, H.L.; Liu, Y.; Fan, F.; Jin, X.F. Non-uniform temperature field and effects of Shanghai 65 m radio telescope. *Opt. Precis. Eng.* **2014**, *22*, 970–978. [CrossRef]
95. McQuiston, F.C.; Parker, J.D.; Spitler, J.D. *Heating, Ventilating and Air Conditioning: Analysis and Design*, 6th ed.; John Wiley and Sons, Inc.: Hoboken, NJ, USA, 2005.
96. Moon, P. Proposed standard solar radiation curves for engineering use. *J. Frankl. Inst.* **1940**, *230*, 583–617. [CrossRef]
97. Threlkeld, J.L.; Jordan, R.C. Direct solar radiation available on clear days. *ASHARE Trans.* **1958**, *64*, 45–48.
98. American Society of Heating, Refrigeration, and Air-Conditioning Engineers. *ASHRAE Handbook of Fundamentals*; American Society of Heating, Refrigeration, and Air-Conditioning Engineers: Atlanta, GA, USA, 1972.
99. Hottel, H.C. A simple model for estimating the transmittance of direct solar radiation through clear atmospheres. *Sol. Energy.* **1976**, *18*, 129–134. [CrossRef]
100. Liu, B.Y.H.; Jordan, R.C. The interrelationship and characteristic distribution of direct, diffuse and total solar radiation. *Sol. Energy.* **1960**, *4*, 1–19. [CrossRef]

101. Kehlbeck, F. *Effect of Solar Radiation on Bridge Structure*; Liu, X.F., Translator; Chinese Railway Publishing Company: Beijing, China, 1981.
102. Dilger, W.H.; Ghali, A.; Chan, M.; Cheung, M.S.; Maes, M.A. Temperature stresses in composite box girder bridges. *J. Struct. Eng.* **1990**, *109*, 1460–1478. [CrossRef]
103. Elbadry, M.M.; Ghali, A. Temperature Variations in Concrete Bridges. *J. Struct. Eng.* **1983**, *109*, 2355–2374. [CrossRef]
104. Chen, Q. Effects of Thermal Actions on Texas Steel Bridges. Ph.D. Thesis, University of Texas at Austin, Austin, TX, USA, 2008.
105. Zhou, M.; Fan, J.S.; Liu, Y.F.; Zhang, J.X.; Duan, X.J.; Lei, S.S. Analysis on non-uniform temperature field of steel girds of Beijing Daxing International Airport terminal building core area considering solar radiation. *Eng. Mech.* **2020**, *37*, 46–54.
106. Zhu, J.; Meng, Q. Effective and fine analysis for temperature effect of bridges in natural environments. *J. Bridge Eng.* **2017**, *22*, 04017017. [CrossRef]
107. Yin, G.S.; Zhao, Z.Y.; Xu, B. Research on temperature field of arch bridge under solar radiation. *Chin. J. Appl. Mech.* **2014**, *31*, 939–944.
108. Chen, Z.; Jin, F.; Wang, J.T. Ray-tracing algorithm for solar radiation intensity computation of arch dam surface. *J. Hydraul. Eng.* **2007**, *38*, 1461–1465.
109. Gohen, M.F.; Greenberg, D.P. The hemi-cube: A radiosity solution for complex environments. *ACM Siggraph Comput. Graph.* **1985**, *19*, 31–40. [CrossRef]
110. Xu, F.; Wang, B.; Zhang, H.L. Improvement upon the formulas for solar position in analysis of sunlight distribution in buildings. *J. Chongqing Jianzhu Univ.* **2008**, *30*, 130–134.
111. Gao, F.; Chen, P.; Xia, Y.; Zhu, H.P.; Weng, S. Efficient calculation and monitoring of temperature actions on supertall structures. *Eng. Struct.* **2019**, *193*, 1–11. [CrossRef]
112. Duffie, J.A.; Beckman, W.A. *Solar Engineering of Thermal Processes*; John Wiley and Sons Inc.: New York, NY, USA, 1980.
113. Liu, N.X.; Qin, Y.G. *Building Thermal Environment*; Tsinghua University Press: Beijing, China, 2005.
114. Lee, J.H. Investigation of Extreme Environmental Conditions and Design Thermal Gradients during Construction for Prestressed Concrete Bridge Girders. *J. Bridge Eng.* **2012**, *17*, 547–556. [CrossRef]
115. Wei, G.P. Research for temperature fields and temperature stresses of prestressed concrete single-box girder bridge. *J. Southwest Jiaotong Univ.* **1989**, *24*, 90–97.
116. Riding, K.A.; Poole, J.L.; Schindler, A.K.; Juenger, M.C.G.; Folliard, K.J. Temperature boundary condition models for concrete bridge members. *ACI Mater. J.* **2007**, *104*, 379–387.
117. Chen, B.B. Study on Heterogeneous Temperature Effect of Large Span Structures under Solar Radiation. Master's Thesis, Tianjin University, Tianjin, China, 2013.
118. Liu, H.B.; Chen, Z.H.; Zhou, T. Theoretical and experimental study on the temperature distribution of H-shaped steel members under solar radiation. *Appl. Therm. Eng.* **2012**, *37*, 329–335. [CrossRef]
119. Zhao, Z.W.; Liu, H.B.; Chen, Z.H. Thermal behavior of large-span reticulated domes covered by ETFE membrane roofs under solar radiation. *Thin Walled Struct.* **2017**, *115*, 1–11. [CrossRef]
120. Xu, Y.L.; Xia, Y. *Structural Health Monitoring of Long-Span Suspension Bridges*; Spon Press: London, UK, 2011.
121. Dilger, W.H. Temperature effects in concrete and composite bridges. In Proceedings of the Workshop on Research and Monitoring of Long Span Bridges, Hong Kong, China; 26–28 April 2000; pp. 1–13.
122. Froli, M.; Hariga, N.; Nati, G.; Orlandini, M. Longitudinal Thermal Behaviour of a Concrete Box Girder Bridge. *Struct. Eng. Int.* **1996**, *6*, 237–242. [CrossRef]
123. Kim, S.H.; Park, S.J.; Wu, J.; Won, J.H. Temperature variation in steel box girders of cable-stayed bridges during construction. *J. Constr. Steel Res.* **2015**, *112*, 80–92. [CrossRef]
124. Wang, G.X.; Ding, Y.L.; Wang, X.J.; Yan, X.; Zhang, Y.F. Long-term monitoring and statistical analysis of temperature field of flat steel-box girder of Sutong bridge. *J. Highw. Transp. Res. Dev.* **2014**, *31*, 69–73.
125. Liu, Y.; Zhang, H.P.; Deng, Y.; Jiang, N.; Zhang, J.R. Temperature field characteristic research of steel box girder for suspension bridge based on measured data. *China J. Highw. Transp.* **2017**, *30*, 56–64.
126. Ding, Y.L.; Wang, G.X.; Zhou, G.D.; Li, A.Q. Life-cycle simulation method of temperature field of steel box girder for Runyang Cable-stayed Bridge based on field monitoring data. *China J. Civ. Eng.* **2013**, *46*, 129–136.
127. Greve, A.; Mangum, J. Mechanical measurements of the ALMA prototype antennas. *IEEE Antennas Propag. Mag.* **2008**, *50*, 66–80. [CrossRef]

128. Bremer, M.; Penalver, J. FE model-based interpretation of telescope temperature variations. *Proc. SPIE* **2002**, *4757*, 186–195. [CrossRef]
129. Greve, A.; Bremer, M.; Penalver, J.; Raffin, P.; Morris, D. Improvement of the IRAM 30-m telescope from temperature measurements and finite-element calculations. *IEEE Trans. Antennas Propag.* **2005**, *53*, 851–860. [CrossRef]
130. Ukita, N.; Ezawa, H.; Ikenoue, B.; Saito, M. Thermal and wind effects on the azimuth axis tilt of the ASTE 10-m antenna. *Publ. Nat. Astron. Obs. Jpn.* **2007**, *10*, 25–33.
131. Ukita, N.; Saito, M.; Ezawa, H.; Ikenoue, B.; Ishizaki, H.; Iwashita, H.; Yamaguchi, N.; Hayakawa, T. Design and performance of the ALMA-J prototype antenna. In Proceedings of the Society of Photo-Optical Instrumentation Engineers, Glasgow, UK, 21–25 June 2004; pp. 1085–1093.
132. Schroeder, D.J. *Astronomical Optics*; Academic Press: San Diego, CA, USA, 1987.
133. Machuyev, Y.I.; Gimmelman, V.G. Temperature state of radio antennas under climatic influences. In Proceedings of the 7th International Symposium on Antennas, Propagation and EM Theory, Guilin, China, 26–29 October 2006; pp. 545–548.
134. Wang, G.X.; Ye, J.H. Localization and quantification of partial cable damage in the long-span cable-stayed bridge using the abnormal variation of temperature-induced girder deflection. *Struct. Control Health Monit.* **2019**, *26*, e2281. [CrossRef]
135. Chen, Z.H.; Chen, B.B.; Liu, H.B. Experimental research on solar radiation absorptance of commonly used coatings for steel structures. *J. Build. Struct.* **2014**, *35*, 81–87.
136. China Architectural & Building Press. *Code for Thermal Design of Civil Building*; GB 50176-2016; China Architectural & Building Press: Beijing, China, 2016.
137. Xiao, X. Experimental and Numerical Study on Temperature of Steel Members and Single-Layer Lattice Shell Considering Coupling of Radiation, Thermal and Fluid. Master's Thesis, Tianjin University, Tianjin, China, 2014.
138. Liu, Y.J.; Liu, J.; Zhang, N. Review on solar thermal actions of bridge structures. *China J. Civ. Eng.* **2019**, *52*, 59–78.
139. Yang, L.; Yang, Z. *Principle and Technology of Temperature Measurement by Infrared Thermography*; Science Press: Beijing, China, 2012.
140. Xing, S.X. *Infrared Thermal Imaging and Signal Processing*; National Defence Industrial Press: Beijing, China, 2011.
141. Ring, E.F.J.; Ammer, K. Infrared thermal imaging in medicine. *Physiol. Meas.* **2012**, *33*, R33–R46. [CrossRef] [PubMed]
142. Bernard, V.; Can, V.; Staffa, E.; Farkasova, M.; Nemcova, M.; Dostal, M.; Kala, Z.; Mornstein, V. Infrared thermal imaging: A potential tool used in open colorectal surgery. *Minerva Chir.* **2017**, *72*, 442–446. [PubMed]
143. Engert, V.; Merla, A.; Grant, J.A.; Cardone, D.; Tusche, A.; Singer, T. Exploring the Use of Thermal Infrared Imaging in Human Stress Research. *PLoS ONE* **2014**, *9*, e90782. [CrossRef] [PubMed]
144. Thanh, N.T.; Sahli, H.; Hao, D.N. Detection and characterization of buried landmines using infrared thermography. *Inverse Probl. Sci. Eng.* **2011**, *19*, 281–307. [CrossRef]
145. Szymanik, B. Inverse Problem Solution in Landmines Detection Based on Active Thermography. *Radioengineering* **2014**, *23*, 1203–1207.
146. Stepanic, J.; Malivovec, M.; Svaic, S.; Krstelj, V. Parameterisation of non-homogeneities in buried object detection by means of thermography. *Infrared Phys. Technol.* **2004**, *45*, 201–208. [CrossRef]
147. Crupi, V.; Chiofalo, G.; Guglielmino, E. Using Infrared Thermography in Low-Cycle Fatigue Studies of Welded Joints. *Weld. J.* **2010**, *89*, 195S–200S.
148. De Brito, J.P.; Henriquez, J.R. Infrared thermography applied for high-level current density identification over planar microwave circuit sectors. *Infrared Phys. Technol.* **2010**, *53*, 84–88. [CrossRef]
149. Meola, C.; Carlomagno, G.M.; Giorleo, L. The use of infrared thermography for materials characterization. *J. Mater. Process. Technol.* **2004**, *155*, 1132–1137. [CrossRef]
150. Cohen, Y.; Alchanatis, V.; Meron, M.; Saranga, Y.; Tsipris, J. Estimation of leaf water potential by thermal imagery and spatial analysis. *J. Exp. Bot.* **2005**, *56*, 1843–1852. [CrossRef]
151. Jones, H.G.; Serraj, R.; Loveys, B.R.; Xiong, L.Z.; Wheaton, A.; Price, A.H. Thermal infrared imaging of crop canopies for the remote diagnosis and quantification of plant responses to water stress in the field. *Funct. Plant Biol.* **2009**, *36*, 978–989. [CrossRef] [PubMed]

152. Lindenthal, M.; Steiner, U.; Dehne, H.W.; Oerke, E.C. Effect of downy mildew development on transpiration of cucumber leaves visualized by digital infrared thermography. *Phytopathology* **2005**, *95*, 233–240. [CrossRef] [PubMed]
153. Barreira, E.; de Freitas, V.P. Evaluation of building materials using infrared thermography. *Constr. Build. Mater.* **2007**, *21*, 218–224. [CrossRef]
154. Cheng, C.C.; Cheng, T.M.; Chiang, C.H. Defect detection of concrete structures using both infrared thermography and elastic waves. *Autom. Constr.* **2008**, *18*, 87–92. [CrossRef]
155. Grinzato, E.; Vavilov, V.; Kauppinen, T. Quantitative infrared thermography in buildings. *Energy Build.* **1998**, *29*, 1–9. [CrossRef]
156. American Association of State Highway and Transportation Officials. *AASHTO LRFD Bridge Design Specifications*; American Association of State Highway and Transportation Officials: Washington, DC, USA, 2017.
157. China Communications Press. *General Specifications for Design of Highway Bridges and Culverts*; JTG D60-2015; China Communications Press: Beijing, China, 2015.
158. British Standards Institution. *Steel, Concrete and Composite Bridges-Part 2: Specification for Loads*; BS 5400-2: 2006; British Standards Institution: London, UK, 2006.
159. Intergovernmental Panel on Climate Change. *Climate Change 2007: The Physical Science Basis*; Cambridge University Press: Cambridge, UK, 2007.
160. Intergovernmental Panel on Climate Change. *Global Warming of 1.5 °C*; Cambridge University Press: Cambridge, UK, 2018.
161. Intergovernmental Panel on Climate Change. *Climate Change 1995: The Science of Climate Change*; Cambridge University Press: Cambridge, UK, 1996.
162. World Meteorological Organization. *The Global Climate in 2015–2019. Research Reports, World Meteorological Organization*; World Meteorological Organization: Geneva, Switzerland, 2020.
163. Fan, Z.; Wang, Z.; Tang, J. Analysis on temperature field and determination of temperature upon healing of large-span steel structure of the National Stadium. *J. Build. Struct.* **2007**, *28*, 32–40.

© 2020 by the authors. Licensee MDPI, Basel, Switzerland. This article is an open access article distributed under the terms and conditions of the Creative Commons Attribution (CC BY) license (http://creativecommons.org/licenses/by/4.0/).